Defining the robust behaviour of the plant clock gene circuit with absolute RNA timeseries and open infrastructure

OPEN BIOLOGY

rsob.royalsocietypublishing.org

Research

Cite this article: Flis A *et al*. 2015 Defining the robust behaviour of the plant clock gene circuit with absolute RNA timeseries and open infrastructure. *Open Biol.* **5**: 150042.
http://dx.doi.org/10.1098/rsob.150042

Received: 30 March 2015
Accepted: 14 September 2015

Subject Area:
systems biology/genetics/bioinformatics/molecular biology

Keywords:
circadian rhythms, plant biology, gene regulatory networks, biological clocks, model optimization, data management

Authors for correspondence:
Mark Stitt
e-mail: mstitt@mpimp-golm.mpg.de
Karen J. Halliday
e-mail: karen.halliday@ed.ac.uk
Andrew J. Millar
e-mail: andrew.millar@ed.ac.uk

†Present address: Biosciences KTN, The Roslin Institute, Easter Bush, Midlothian EH25 9RG, UK.
‡Present address: NUIG, Plant Systems Biology Laboratory, Plant and AgriBiosciences Research Centre, Botany and Plant Science, Galway, Ireland.

Electronic supplementary material is available at http://dx.doi.org/10.1098/rsob.150042.

THE ROYAL SOCIETY PUBLISHING

Defining the robust behaviour of the plant clock gene circuit with absolute RNA timeseries and open infrastructure

Anna Flis[1], Aurora Piñas Fernández[2,†], Tomasz Zielinski[2], Virginie Mengin[1], Ronan Sulpice[1,‡], Kevin Stratford[3], Alastair Hume[2,3], Alexandra Pokhilko[2,4], Megan M. Southern[5], Daniel D. Seaton[2], Harriet G. McWatters[2], Mark Stitt[1], Karen J. Halliday[2] and Andrew J. Millar[2]

[1]Max Planck Institute of Molecular Plant Physiology, Am Muehlenberg 1, 14476 Potsdam-Golm, Germany
[2]SynthSys and School of Biological Sciences, University of Edinburgh, C.H. Waddington Building, Edinburgh EH9 3JD, UK
[5]EPCC, University of Edinburgh, James Clerk Maxwell Building, Edinburgh EH9 3JZ, UK
[6]Institute of Molecular Cell and Systems Biology, University of Glasgow, Bower Building, Glasgow G12 8QQ, UK
[7]Department of Biological Sciences, University of Warwick, Coventry CV4 7AL, UK

AJM, 0000-0003-1756-3654

Our understanding of the complex, transcriptional feedback loops in the circadian clock mechanism has depended upon quantitative, timeseries data from disparate sources. We measure clock gene RNA profiles in *Arabidopsis thaliana* seedlings, grown with or without exogenous sucrose, or in soil-grown plants and in wild-type and mutant backgrounds. The RNA profiles were strikingly robust across the experimental conditions, so current mathematical models are likely to be broadly applicable in leaf tissue. In addition to providing reference data, unexpected behaviours included co-expression of *PRR9* and *ELF4*, and regulation of *PRR5* by *GI*. Absolute RNA quantification revealed low levels of *PRR9* transcripts (peak approx. 50 copies cell^{-1}) compared with other clock genes, and threefold higher levels of *LHY* RNA (more than 1500 copies cell^{-1}) than of its close relative *CCA1*. The data are disseminated from BioDare, an online repository for focused timeseries data, which is expected to benefit mechanistic modelling. One data subset successfully constrained clock gene expression in a complex model, using publicly available software on parallel computers, without expert tuning or programming. We outline the empirical and mathematical justification for data aggregation in understanding highly interconnected, dynamic networks such as the clock, and the observed design constraints on the resources required to make this approach widely accessible.

1. Introduction

Circadian clocks are found widely among organisms from archaea to mammals [1,2]. These internal time-keepers generate approximately 24 h rhythms in the expression of 10–30% of genes, even without environmental cues. In natural conditions, circadian rhythms are entrained by light and temperature cycles. Their function is to coordinate internal processes with the external day/night cycle [3,4] and also, through photoperiodism, relative to the seasonal cycle [5]. The circadian system of each organism includes a phylum-specific gene regulatory network that is required for most rhythmicity [6], as well as non-transcriptional oscillator(s) that are less well characterized in eukaryotes [7].

In plants, the clock gene network includes highly connected, negative regulators forming a complicated circuit. This has been best studied in *Arabidopsis thaliana*. One simplification (figure 1*a*) visualizes the circuit as a three-loop

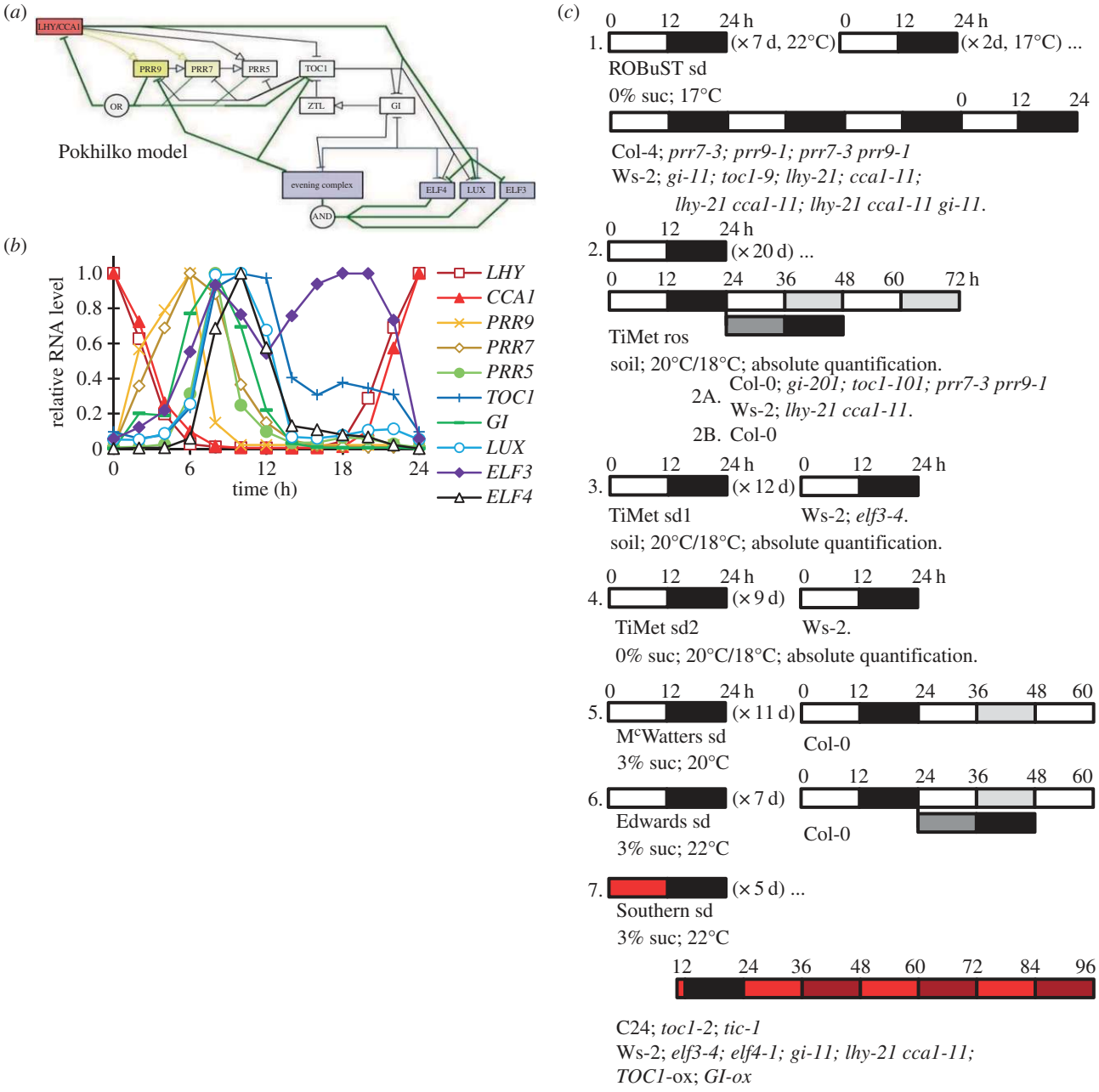

Figure 1. The clock gene network and experimental protocols. (*a*) The clock gene network summarized in the activity-flow language of SBGN v. 1.0 [8], with the principal connections in the P2012 model [9]. The repressilator is denoted by green lines; morning loop components are filled yellow; *LHY/CCA1*, red; evening loop components, blue. Light inputs are shown in electronic supplementary material, figure S1 and all modelled connections of P2011 [10] in electronic supplementary material, figure S2. (*b*) Peak-normalized RNA profiles of genes depicted in (*a*), in plants of the Col-0 accession under a 12 h light : 12 h dark cycle (LD 12 : 12; experiment 2*b* of panel (*c*)). (*c*) Graphical representation of the growth conditions. Experiments 1, 4, 5, 6 and 7 used seedlings grown in LD 12 : 12 for the number of days indicated; experiments 2 and 3 used plants grown on soil in LD 12 : 12 for the number of days indicated. Sucrose concentrations, growth temperatures and genotypes tested are shown for each experiment. Open box, light interval; black box, dark interval; light grey box, predicted darkness in constant light; dark grey box, predicted light in constant darkness; red box, red light. Sampling time in ZT (h), relative to lights-on of the first day of sampling or the last dawn before experimental treatment (ZT0). Ros, rosette; sd, seedling.

structure of morning and evening loops coupled around a repressilator [10,11]. The morning loop includes the MYB-related transcription factors LHY and CCA1, which activate expression of the pseudo-response regulators *PRR9* and *PRR7* [12,13], but inhibit expression of later-expressed genes including *PRR5* and *TOC1* (*PRR1*). PRR9, PRR7, PRR5 and TOC1 bind to and inhibit *LHY* and *CCA1* expression, as predicted by modelling [10,14] and demonstrated by experiments [15–18]. LHY and CCA1 also inhibit expression of *ELF3*, *ELF4* and *LUX* (*PCL1*), whose protein products interact to form another repressor, the evening complex (EC) [19–22]. The EC is thought to inhibit the expression of at least *ELF4* and *LUX*, forming a negative feedback loop, whose continued function might explain the damped oscillation of clock gene expression observed in *lhy cca1* double mutant plants [10]. GI, a large plant-specific protein, is also rhythmically expressed but functions at a post-translational level through, for example, stabilization of the TOC1-degradation factor ZTL [23]. Light signalling controls multiple processes (electronic supplementary material, figure S1) that entrain the clock circuit to the day–night cycle. A growing number of identified processes and components remain to be fully integrated into the circuit, though even the components described are challenging to analyse.

Formal, mathematical models have been helpful in understanding the plant clock, because its components are highly interconnected by nonlinear regulation (electronic supplementary material, figure S2; reviewed in [24]). Model development was necessarily based upon timeseries data, where the system was manipulated using mutations and by varying light or temperature inputs. More detailed models demanded greater precision and breadth in the data, which raised two major issues. First, data collation was laborious, because the numerical data underlying published timeseries graphs were rarely accessible [25]. Although the potential benefits of data sharing are recognized [26,27], in practice, useful sharing requires cyber infrastructure, which is currently best-developed for omics data rather than the many focused studies in the clock literature [28]. Second, the published data on *Arabidopsis* clocks used several genetic backgrounds and growth conditions, introducing ill-defined variation to the results.

To provide directly comparable data, we conducted large-scale qRT-PCR assays for the RNA levels of multiple clock genes. Overlapping studies in four laboratories using different growth stages and conditions highlighted the robustness of most expression profiles and the few instances where they varied. Visualizing the data as phase plane plots suggested new dynamic interactions and their genetic regulators. Absolute RNA quantification revealed the low expression levels of *ELF3* and *PRR9*. To facilitate similar projects, we introduce data aggregation in the online BioDare resource, and illustrate the utility of our datasets by reoptimizing the P2011 clock model [10] with the open-source application Systems Biology Software Infrastructure (SBSI) [29], highlighting key areas for future experiments.

2. Results

2.1. Large-scale measurement of clock gene RNA profiles

This study was motivated by two projects that integrated circadian regulation into research on other plant physiological systems, which were incompatible with the growth conditions used in earlier circadian research. The Regulation of Biological Signalling by Temperature (ROBuST) project studied the interactions of ambient temperature with circadian and light signalling circuits; exogenous sucrose inhibits light signalling [30,31] and was therefore excluded. The Timing of Metabolism (TiMet) project studied circadian regulation of the starch pathway, among others, which is best characterized in rosette plants grown on soil. To measure the rhythmic expression in a set of clock-related genes (figure 1*b*), we used automated systems in Golm and Edinburgh to quantify mRNA levels for components of the clock circuit every 2 h, in multiple conditions and mutant backgrounds [32,33] (figure 1*c*). The ROBuST dataset tested 13-day-old, wild-type (WT) and mutant seedlings grown at 17°C on agar medium without additional sucrose. Datasets from the TiMet project tested 21-day-old rosette plants grown at 20°C on soil (TiMet ros) and 13-day-old seedlings on soil (TiMet sd1). The TiMet rosette data were collected from WT and clock mutant *Arabidopsis thaliana* plants grown under light : dark (LD) cycles in two experiments, followed by constant light (LL) or constant dark (DD) in one study. Three further studies were compared, from seedlings grown on sterile agar media without sucrose (TiMet sd2, using the same medium as the ROBuST data), or with exogenous sucrose under white (McWatters, this paper; and Edwards *et al*. [34]) or red light (Southern, this paper; and [21,35]).

2.2. Data presentation

Time is expressed as zeitgeber time (ZT) in hours since the last dark–light transition, by convention; the first dark–light transition within the sampling interval is 0 h on our plots. TiMet data are presented as absolute values [33], obtained by calibrating RNA extraction efficiency with heterologous control RNAs (electronic supplementary matetial, table S1) to calculate the number of copies of each RNA per gram fresh weight (gFW). Estimated cell numbers per gFW (see electronic supplementary material) were used to calculate RNA copies per cell. The other datasets are normalized relative to a control transcript (*ACTIN7* for ROBuST; *ACTIN2* for Edwards and Southern; *βTUBULIN4* for McWatters). *ACTIN2* and *GAPDH* controls were also assayed with two amplicons each in the TiMet assays, for comparison among datasets. Data were replicated in biological duplicate or triplicate samples and in equivalent sampling on successive days (0–12 h and 24–36 h in the TiMet and Edwards datasets). Data are presented on linear scales to reflect the potential for protein synthesis and hence regulatory effects on downstream targets (in keeping with most of the literature; figures 2 and 3; electronic supplementary material, figure S5) and on logarithmic scales to reveal the full dynamic range of RNA expression, and hence the influence of multiple upstream regulators (figures 4–6; electronic supplementary material, figure S3 and S4). Further technical comparison among the studies is presented in the electronic supplementary material.

2.3. Similarity and specific variations of wild-type RNA profiles across datasets

Clock gene RNA expression profiles in WT plants of two accessions (Col and Ws-2) grown in LD are presented in figure 2; profiles were similar across the TiMet and ROBuST datasets, despite major differences in growth conditions. The morning clock components, *CCA1* and *LHY*, peaked as expected at dawn (figure 2*a*,*b*), followed by *PRR7* (ZT6; figure 2*c*,*d*), *PRR5* and *GI* (ZT8; figure 2*e*–*h*). Expression of the evening components, *LUX*, *ELF4* and *TOC1*, peaked at ZT8–12 (figure 2*e*–*j*); peak expression of *LUX* was delayed by about 2 h in Col plants relative to Ws-2 in both datasets (figure 2*g*,*h*; replicated in LL data). *ELF3* had a low-amplitude profile in both datasets, with lowest expression around ZT4.

The TiMet and ROBuST datasets differed at particular timepoints for *PRR9*, *GI* and *TOC1*. *PRR9* expression was highest at ZT2–6 in both cases, with a clear peak at ZT2 in the ROBuST seedling data (consistent with many other reports from seedlings) but a broader profile in the TiMet data (figure 2*c*,*d*). After its major peak at ZT8–12, *TOC1* expression is consistently observed (since [36]) to increase around ZT18, but the level of this night-time peak varied (figure 2*e*,*f*). The ROBuST data for seedlings showed a peak of *GI* expression at ZT2 (figure 2*f*); little induction is evident at ZT2 in the TiMet rosette data on a linear scale (figure 2*e*) though the logarithmic scale reveals the response (electronic supplementary material, figure S3*e*). The morning peak in

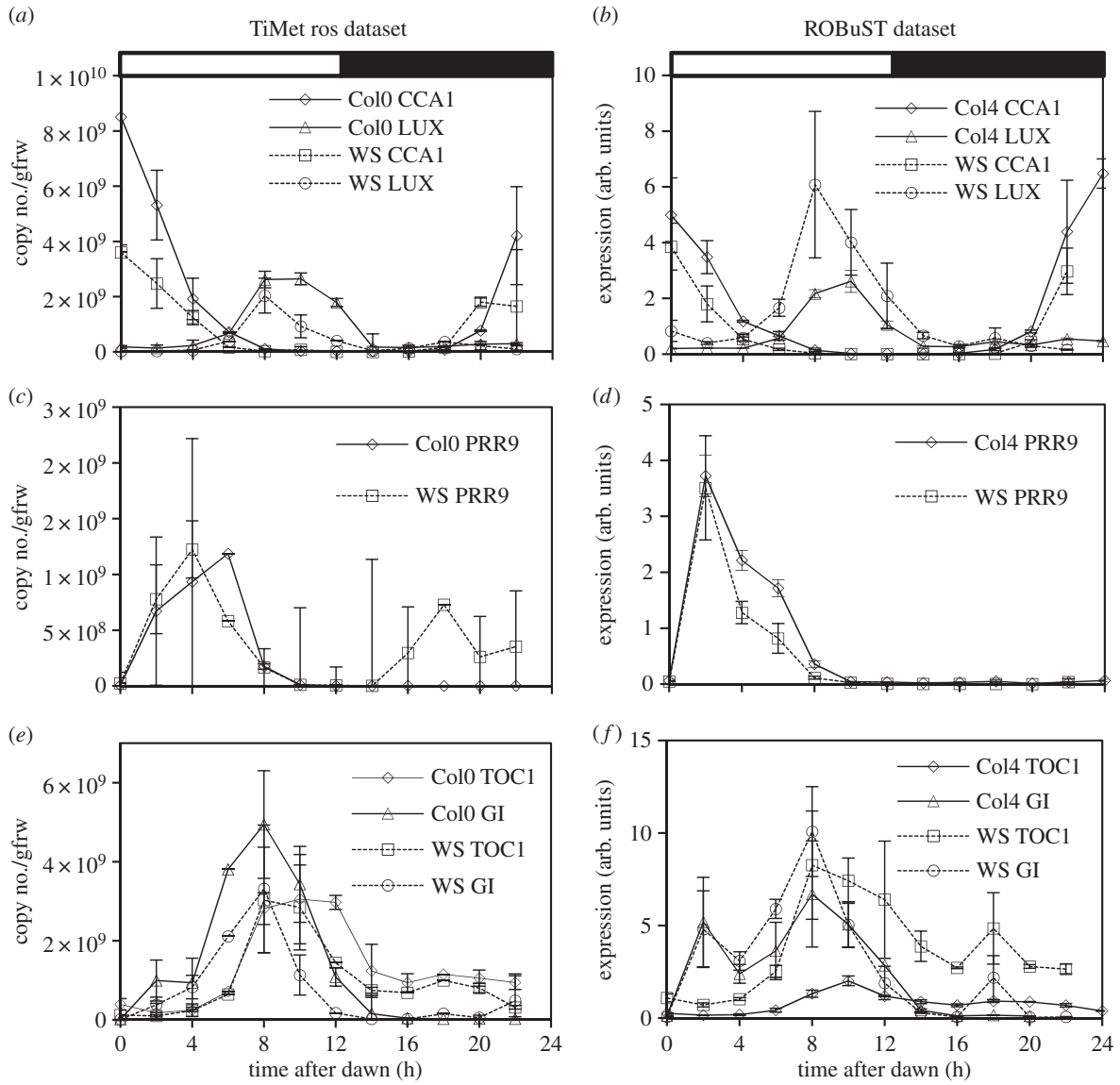

Figure 2. Clock gene expression in wild-type plants under LD cycles. Transcript levels in Col-0 and Ws-2 WT under LD 12 : 12 were measured by qRT-PCR, in experiment 2 (TiMet ros) including eight external RNA standards to allow absolute quantification in Col-0 and Ws-2 (*a,c,e*) and in experiment 1 (ROBuST) normalized to the *ACTIN7* control in Col-4 and Ws-2 (*b,d,f*). Data represent transcripts of (*a,b*) *LHY* and *CCA1*, (*c,d*) *PRR9*, and (*e,f*) *TOC1* and *GI*. Error bars show SD, for two to three biological replicates. Electronic supplementary material, figure S3 shows the data on logarithmic plots.

GI is likely to be an acute response to lights-on. Rapid sampling in the Southern data [35] and in a follow-up microarray study [10] suggested that induction is rapid but transient, and therefore sensitive to sampling time. Nonetheless, the data suggest that either the magnitude or kinetics of light responsiveness vary across the conditions tested. The difference in *PRR9* profiles could reflect slower activation of *PRR9* in the TiMet data, consistent with lower light responsiveness in rosettes than in seedlings or with faster repression of *PRR9* in seedlings. The level of *GI* transcripts at ZT12 also varied from 4% to 40% of the peak level, with the lowest level in rosettes of Ws-2 (figures 2*e,f* and 3*c*). *GI* expression is light sensitive at this phase [37], so our results are consistent with variation in light responsiveness.

Sucrose modestly increases expression of the evening clock components *TOC1* and *GI* [38], particularly in darkness [39], and can repress *PRR7* with subsequent effects on *CCA1* under low light [40], along with transcriptome-wide effects under LD cycles [41,42]. We therefore compared the expression profiles for *CCA1*, *TOC1* and *GI* in plants grown without (ROBuST and TiMet data) or with exogenous sucrose (McWatters, Edwards and Southern datasets; figure 3). To facilitate comparison, TiMet data were normalized to control transcripts (two amplicons each in *GAPDH* and *ACTIN2*), as for the other studies. Each profile was normalized to its maximum. Expression profiles of *CCA1* across the different timeseries matched closely despite the differences in accession and experimental protocols (figure 3*a*). The times of peak, mid-rising and mid-falling phases differed by at most 2 h (one sampling interval) among datasets. In the falling phase at ZT4, the profiles in McWatters, TiMet ros and TiMet sd2 data were delayed relative to the other data. The night-time expression of *TOC1* at ZT18 varied from 20% to 60% of the main peak level (figure 3*b*), with high expression in ROBuST, Edwards and TiMet sd2 datasets. The expression of *GI* at ZT2 in the TiMet and Edwards seedling data was about 20% of the main peak level (figure 3*c*, also in Southern data [35]), intermediate between the levels in ROBuST and TiMet rosette data (discussed above). These features of the expression profiles showed no clear relationship with growth medium or developmental stage.

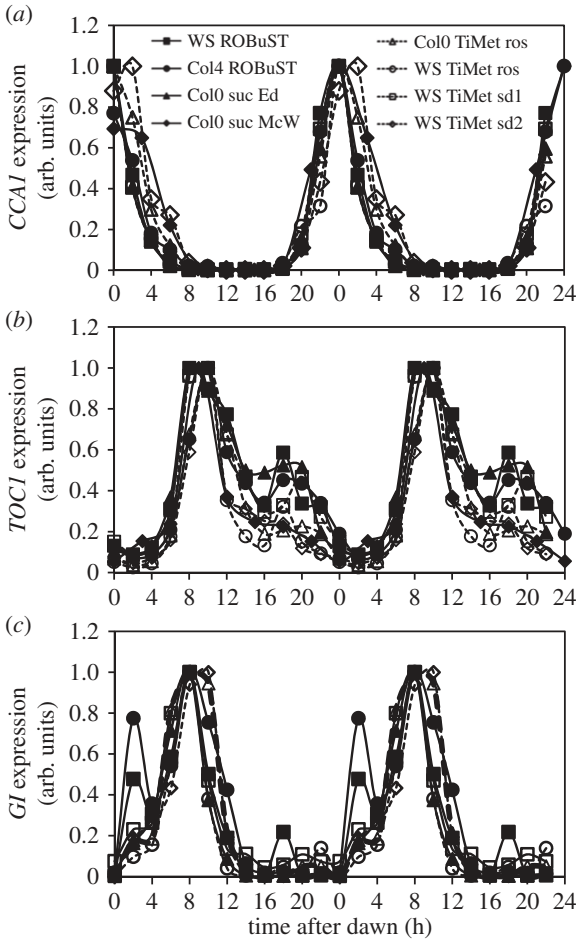

Figure 3. Waveforms of clock gene expression across experiments at different plant age and in the absence and presence of exogenous sucrose. This plot compares transcript abundance of *CCA1*, *TOC1* and *GI* in 12 h photoperiods in three WTs grown in different experimental conditions in different laboratories. The data are taken from the following experiments (figure 1): WS ROBuST (1, seedlings), Col4 ROBuST (1, seedlings), Col0 suc Ed (6, seedlings provided with 3% exogenous sucrose), Col0 suc McW (5, seedlings provided with 3% sucrose), Col0 TiMet ros (2B, 21 day-old rosettes), WS TiMet ros (2, 21 day-old rosettes), WS TiMet sd1 (3, 10 day-old seedlings), WS TiMet sd2 (4, 13-day-old seedlings). All plants were entrained in LD 12 : 12 (figure 1). Values for each transcript are normalized to the peak. The results are the mean of duplicate or triplicate samples, double-plotted; error bars are not shown for clarity.

2.4. Absolute quantification of clock gene transcripts

The absolute quantification in the TiMet ros data, which is based ultimately upon the certified amounts of synthetic commercial standards [33], revealed wide variation in peak RNA levels among clock genes in WT plants (figure 4). Highest RNA levels were detected for *LHY* at 1000–2100 copies per cell, similar to the control genes *GAPDH* and *ACT2*. *PRR9* was least abundant at the peak, with 40–70 copies per cell; *LUX* and *ELF3* peaked at 105–130 copies per cell; *PRR7*, *PRR5*, *GI* and *TOC1* at 120–270 copies per cell; *ELF4* and *CCA1* at 250–600 copies per cell. RNA copy number of *LHY* was threefold greater than that of *CCA1* (figure 4*a*,*b*).

Peak levels for the evening-expressed genes (figure 4*f*–*j*) were slightly higher in Ws-2 than Col-0 plants, by 1.2-fold (*LUX*) to 2.0-fold (*ELF4*), average 1.6-fold. Several clock gene RNAs fell to low copy numbers per cell at the trough. Consequently, rhythmic amplitudes (defined here as peak divided by trough levels) also varied greatly among clock genes. The *TOC1* and *ELF3* profiles showed only eight- to 20-fold amplitude in Col-0, and generally smaller amplitudes in other, mutant genotypes than the other clock genes (figure 4*f*,*i*), whereas *LHY*, *CCA1*, *GI*, *ELF4* and *PRR5* RNAs showed over 100-fold amplitude. This distinction was consistent in other datasets [21,34]. Amplitude estimates can be significantly affected by variation in the very low trough levels, which were higher in the TiMet sd1 dataset relative to the TiMet rosette data for *LHY* and all the evening-expressed genes in the Ws-2 accession, for example (figure 4). Transcripts with high-amplitude profiles might be expected to control circadian timing more effectively than the low-amplitude profiles of *TOC1* and *ELF3*.

2.5. Regulation of clock genes under environmental and genetic manipulation

The TiMet project measured clock gene expression in LL and DD following LD entrainment, in seedlings of two WT and four clock mutant backgrounds (figure 5), revealing novel aspects of clock gene regulation as well as replicating regulation observed in many earlier, smaller studies. The results are discussed below with respect to the upstream regulators of each gene, rather than the effect on the gene's downstream targets. The RNA data are therefore presented in semi-logarithmic plots that show regulator activity even at low RNA levels.

Comparing the three environmental conditions, peak RNA expression levels tended to fall in LL, consistent with the loss of dark-dependent regulation. The acute gene induction at the dark–light transition, faster degradation of PRR repressors in darkness and of the EC in the light are all expected to enhance rhythmic amplitude in LD. Expression levels of the clock RNAs were maintained in the first cycle in DD, except for the strongly light-regulated *ELF4* [43,44]. Comparing the six genotypes, mutations that removed the repressors revealed the key connections in the clock circuit (figure 1*a*). The *gi* mutation, in contrast, had small or negligible effects on the timing and levels of expression except for *PRR5*, as noted below.

2.5.1. *LHY* and *CCA1*

Our results are consistent with PRR repressors controlling both the rising and falling phases of *LHY* and *CCA1* expression at the transcriptional level [14,16–18,45]; several observations suggest that this activity is light-dependent. Both transcripts retain strikingly higher expression in the *prr7;prr9* double mutant than in the WT, at ZT6–12 in LD and LL (figure 5*a*,*b*; $p < 0.05$; 20- to 30-fold higher at ZT8), consistent with the absence of repression from PRR9 and PRR7 proteins. By the second day in LL, the trough of *LHY* and *CCA1* expression at ZT44 (68 h in figure 5) was also 20-fold higher than the WT trough level at ZT36–38 (60–62 h). Comparing LD and LL data with DD conditions revealed broader peaks of *LHY* and *CCA1* RNA in DD (figure 5*k*,*l*), consistent with slower degradation of these transcripts in darkness [34,46]. In darkness, however, *LHY* and *CCA1* levels in the *prr7;prr9* mutant behaved very similarly to the WT, both during the falling phase in DD (ZT28–38; figure 5*k*,*l*) and during the rising phase in LD (ZT16–22; figure 5*a*,*b*). By dawn in LD, both transcripts peaked at the WT level, consistent with previous reports

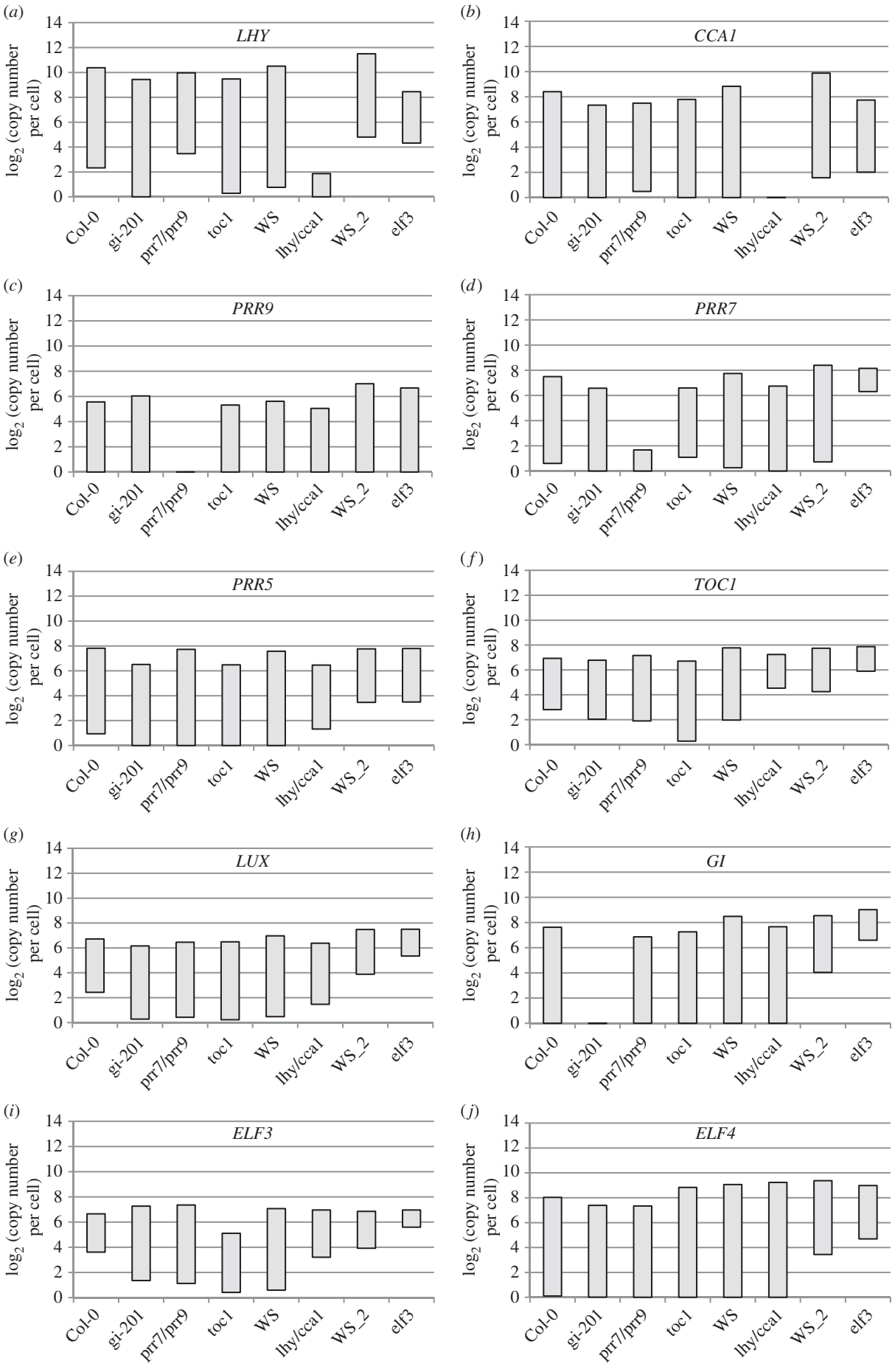

Figure 4. Range of transcript abundance for clock genes in clock mutants. The bars show the highest and lowest mean values for the absolute abundance of transcripts for clock genes in a given genotype. The genotypes are, from left to right, Col-0 wild-type, *gi-201*, *prr9 prr7* double mutant, *toc1*, WS WT, *lhy cca1* double mutant (from experiments 2 and 2B of figure 1*c*, 21-day-old rosettes) and WS (designated WS_2) and *elf3* from experiment 3 (13-day-old seedlings), (*a*) *LHY*, (*b*) *CCA1*, (*c*) *PRR9*, (*d*) *PRR7*, (*e*), *PRR5*, (*f*), *TOC1*, (*g*) *LUX*, (*h*) *GI*, (*i*) *ELF3*, (*j*) *ELF4*. The underlying data are as in figures 5 and 6.

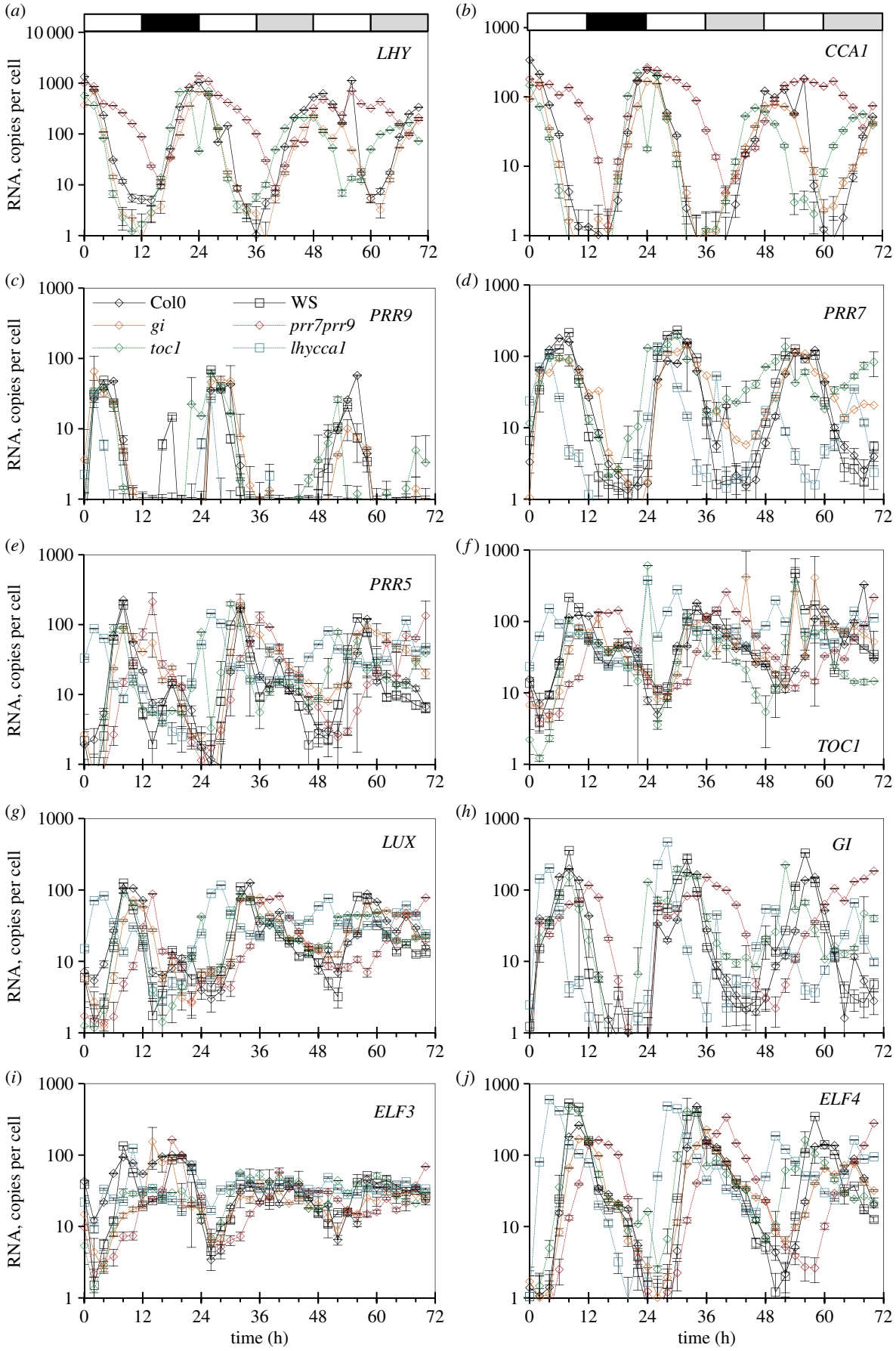

Figure 5. Clock gene expression in wild-type plants and clock mutants in LD, and after transition to constant light (LL) or darkness (DD). Col-0 and Ws-2 WT, the *lhy-21 cca1-11* and *prr7-3 prr9-1* double mutants, and the *toc1-101* and *gi-201* single mutants were grown in a 12 h photoperiod for 20 days, harvested through a LD cycle and then transferred to LL (*a–j*) or DD (*k–t*; TiMet ros, dataset 2 of figure 1*c*). Transcript levels for clock genes were measured by qRT-PCR, including eight external RNA standards to allow absolute quantification. (*a,k*) *LHY*, (*b,l*) *CCA1*, (*c,m*) *PRR9*, (*d,n*) *PRR7*, (*e,o*), *PRR5*, (*f,p*), *TOC1*, (*g,q*) *LUX*, (*h,r*) *GI*, (*i,s*) *ELF3*, (*j,t*) *ELF4*. The results are the mean of duplicate samples, error bars show SD. Open box, light interval; black box, dark interval; light grey box, predicted darkness in LL; dark grey box, predicted light in DD.

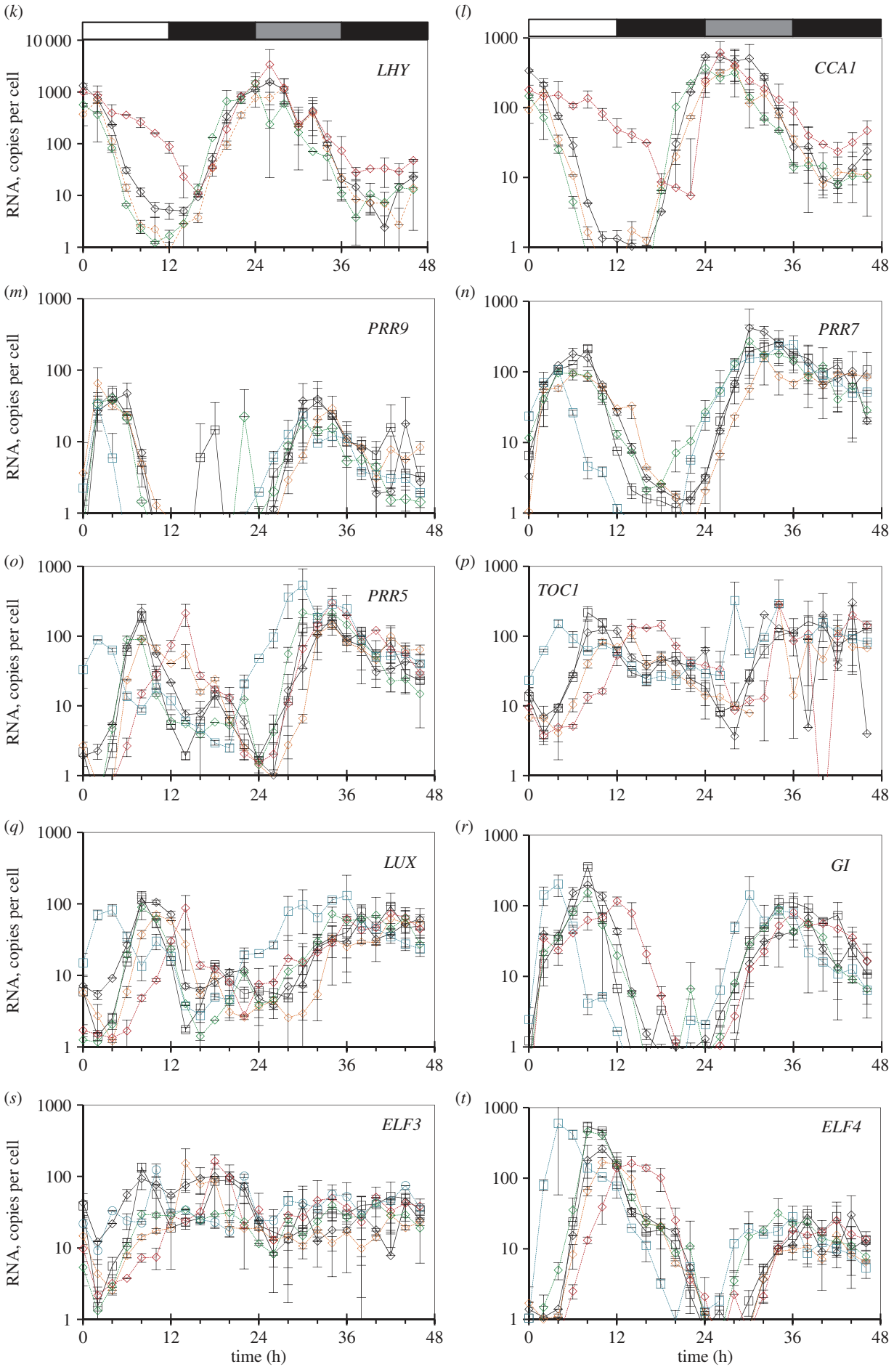

Figure 5. (*Continued.*)

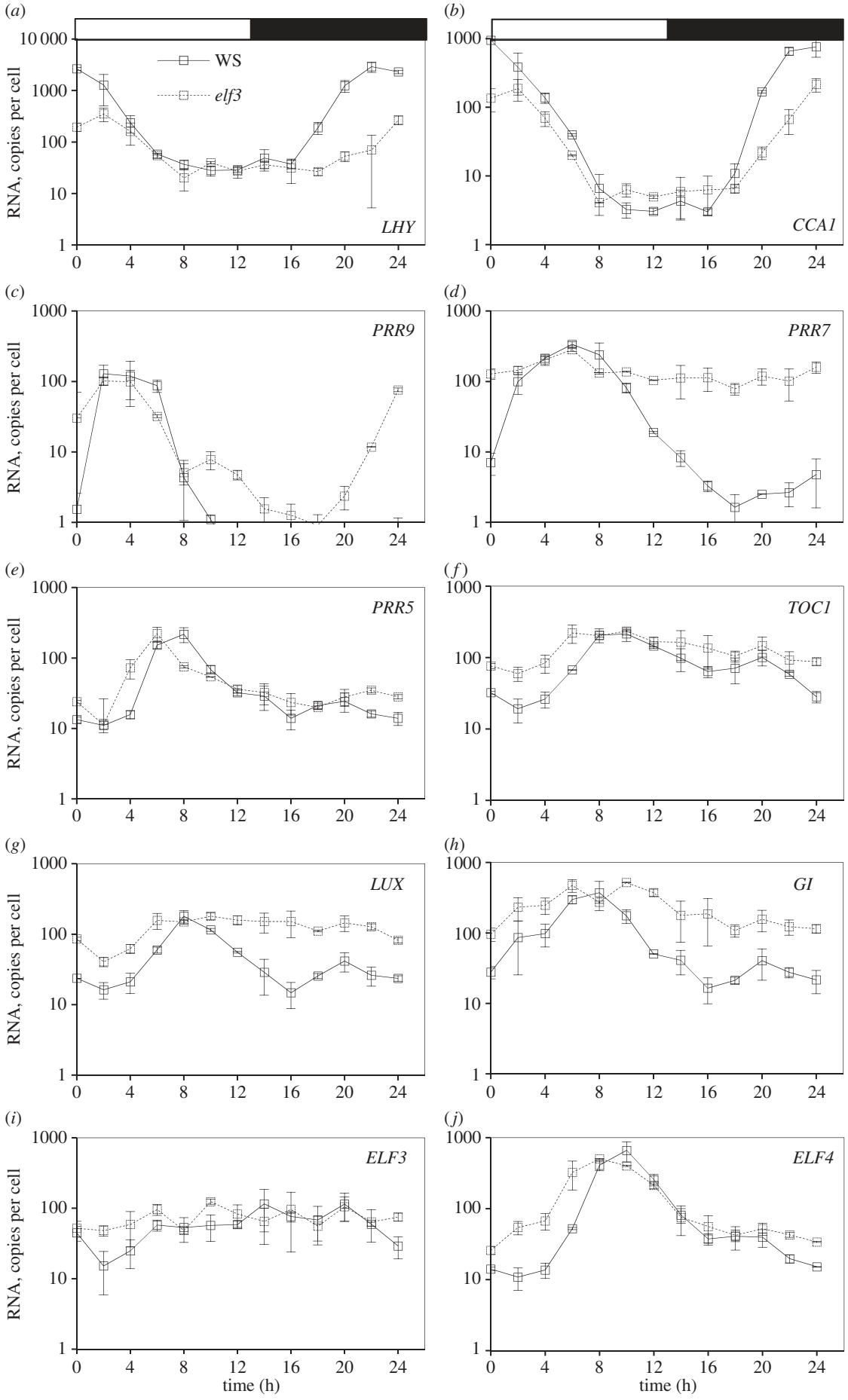

Figure 6. Clock gene expression in wild-type plants and *elf3* mutants in LD. Ws-2 WT (solid lines) and *elf3–4* mutant plants (dashed lines) were grown in a 12 h photoperiod for 12 days and harvested through one LD cycle (TiMet sd, dataset 3 of figure 1*c*). Transcript levels for clock genes were measured by qRT-PCR, including eight external RNA standards to allow absolute quantification. (*a*) *LHY*, (*b*) *CCA1*, (*c*) *PRR9*, (*d*) *PRR7*, (*e*), *PRR5*, (*f*), *TOC1*, (*g*) *LUX*, (*h*) *GI*, (*i*) *ELF3*, (*j*) *ELF4*. The results are the mean of duplicate samples. Error bars show SD.

[12,13]. Thus, the misregulation of *LHY* and *CCA1* in the light in the *prr7;prr9* double mutant was abolished during the dark in LD.

Removing TOC1, the last of the PRR repressors to be expressed, would be expected to allow an earlier rise in expression of *LHY* and *CCA1* during the night in the *toc1* mutant under LD. This effect was relatively small (two- to 2.5-fold higher at ZT18, $p = 0.02$). *LHY* and *CCA1* levels in *toc1* mutants differed less than fourfold from WT at any point in LD. The mutant phenotype was not enhanced in the first DD cycle (figure 5*k*,*l*). In LL, however, *LHY* and *CCA1* expression in the *toc1* mutant peaked at ZT22 (46 h in figure 5) rather than at ZT26 (50 h) in Col, reached only 30–50% of WT peak level consistent with earlier data [47], and fell much earlier than the WT (19- to 27-fold lower at ZT30, time 54 h in figure 5*a*,*b*). Thus, the molecular phenotypes of both *prr7;prr9* and *toc1* mutants were light-dependent.

The *elf3* mutant reduced peak expression of both *LHY* and *CCA1* by five- to 10-fold (figure 6*a*,*b*; electronic supplementary material, figure S5*g*), with greatest effects at ZT20–24. This effect is thought to be indirect, as the EC (comprising ELF4, ELF3 and LUX) is proposed to repress the *PRR*s (figure 1*a*), as well as *LUX* and *ELF4* [10,19,20,22]. De-repression of *PRR* expression in mutants of the EC should therefore explain the effects of *elf3* on *LHY* and *CCA1*.

2.5.2. *PRR9* and *PRR7*

PRR7 was the most severely affected gene in the *elf3* mutant under LD, maintaining 25–85% of the WT peak level at all times (figure 6*d*), consistent with de-repression of the *PRR7* promoter [21]. The resulting, 30- to 50-fold overexpression of *PRR7* in *elf3* at ZT20–24 is consistent with reduced expression of *LHY* and *CCA1* at this time. *PRR9* transcript levels retained a 100-fold rhythmic amplitude under LD in the *elf3* mutant, indicative of ELF3-independent regulation (see Discussion). Nonetheless, *PRR9* expression was also de-repressed from ZT10 in *elf3* ($p = 0.05$), rising 2–4 h before dawn (figure 6*c*), and presumably also contributing to reduce *LHY* and *CCA1* expression.

The early-expressed *PRRs* are thought to be repressed by the later-expressed *PRR5* and *TOC1* (figure 1*a*). The *toc1* mutation had modest effects on *PRR9* or *PRR7* profiles under LD cycles (figure 5*c*,*d*), though the changes observed (such as an early rise in *PRR7* at ZT20–24) were not consistently significant in the TiMet and ROBuST datasets, or in DD in the TiMet data (figure 5*n*). *toc1* also had little effect on *LHY* and *CCA1* levels in these conditions (figure 5*a*,*b*). In LL, however, removing TOC1 prevented full repression of the *PRR*s. The trough of *PRR7* expression was at a 10-fold higher level than in the WT ($p < 0.05$) and 8 h earlier (ZT12 rather than ZT20, 36 h rather than 44 h in figure 5*d*). Higher expression of the repressor *PRR7* at 38–52 h (figure 5*d*) is consistent with the lower peak expression of *CCA1* and *LHY* in *toc1* under LL (figure 1*a* [9]). Taken together, these results suggested that TOC1 repressor function was most effective under constant light conditions, where the *toc1* mutant was originally identified [48].

Light-dependent regulation was also evident in WT plants. Peak *PRR9* expression levels fell less than twofold in the first cycle of DD ($p > 0.16$; figure 5*m*). Peak *PRR7* expression tended to increase (threefold or less) in all genotypes in DD (figure 5*n*; electronic supplementary material, figure S4*c*). The *gi* mutant was an exception, which slowed the rise of all the transcripts in DD except *ELF3* and *ELF4* (figure 5*k–t*; electronic supplementary material, figure S5*d*). Peak expression for some genes was reduced in *gi* below WT levels, including *PRR7* ($p = 0.02–0.03$ at ZT26–28 h). Trough RNA levels in the WT plants rose more dramatically in DD, for *PRR7* and other clock genes (except for *LHY*): the lowest expression of *PRR7* in Col was 1.5 ± 0.4 copies per cell at ZT20 but 65 ± 6.8 copies per cell at ZT40 (electronic supplementary material, figure S4*c*). The Edwards dataset showed similar de-repression of *CCA1* and *GI* trough levels in DD (electronic supplementary material, figure S4*a*,*b* [34]). Lastly, we tested the effect of CCA1 and LHY on the *PRR* transcripts, using the *lhy;cca1* double mutant. In the WT, the repression of the evening-expressed genes by LHY and CCA1 in the early day delays the expression of these and other target genes until the evening. The double mutation advanced the peak phase of all the other clock genes to ZT2–4, as expected, except for *ELF3* (see below). Despite the de-repression, peak levels were not consistently increased relative to the Ws-2 control. Peak expression of *PRR9*, *PRR7* and *PRR5* (figure 5*c–e*) was slightly reduced (up to twofold) in the *lhy;cca1* background under LD, consistent with earlier results [12]. By ZT8 (or ZT4 for *PRR9*), all the clock genes were expressed at lower levels in *lhy;cca1* than in the WT ($p < 0.01–0.04$), consistent with expression of all the PRR repressors. In the *lhy;cca1* double mutant in DD, however, the *PRR* genes had broad peaks that rose earlier than in the WT (ZT22–30) but did not fall earlier (ZT34–40; figure 5*m–o*; electronic supplementary material, figure S4*d*). The absence of early repression in DD again suggests that inter-regulation of the *PRR*s is light-dependent.

2.5.3. *PRR5* and *TOC1*

The later-expressed *PRR*s are repressed by LHY and CCA1, so longer expression of *LHY* and *CCA1* in the *prr7;prr9* double mutants delayed their expression in LD and LL conditions (figure 5*e*,*f*), as expected. In contrast, under DD conditions, *PRR5* expression in *prr7;prr9* rose indistinguishably from the WT at ZT26–34 h and peaked slightly (twofold) above the WT level (figure 5*o*). The *lhy;cca1* double mutant caused the phase advance noted above, as the loss of LHY and CCA1 repressors increased *TOC1* levels in the early day. Peak *TOC1* RNA levels in the *lhy;cca1* mutant did not change consistently from WT levels in the TiMet data under LD (figure 5*f*), and were lower than the WT in the ROBuST dataset ($p < 0.01$; electronic supplementary material, figure S5*c*).

Our detailed datasets also allowed us to compare expression waveforms. For example, *PRR5* rises and falls 10-fold within 5 h in both TiMet and ROBuST data (figure 5*e*,*o*; electronic supplementary material, figures S3*g*,*h*, S5*a*). This narrow peak indicates highly nonlinear control, consistent with negative autoregulation and/or inhibition by TOC1 [15,49]. Moreover, our results indicate that this *PRR5* waveform depends upon GI function. The *gi-201* mutant had limited effects overall but slowed the fall in *PRR5* mRNA in LD and LL (figure 5*e*), creating an asymmetric profile in *PRR5* RNA that was also observed in the *gi-11* tested in the ROBuST data (electronic supplementary material, figure S5*a*,*b*). Repression by the EC might also contribute to the falling phase of the *PRR5* profile. Removing this repression in the *elf3* mutant resulted in moderate de-repression of *PRR5* and *TOC1* in the

late night ($p < 0.01$, ZT0/24; $p = 0.01$ for *PRR5* ZT22) and potentially in the early morning ($p = 0.06$–0.08; ZT2–4; figure 6*e*,*f*). In contrast, de-repression of the early *PRR*s in *elf3* was greatest in the early night (see above), indicating that the profile of regulators varies among the PRR family members (see Discussion).

2.5.4. *GI*

The main peak of *GI* expression in the late day behaves similarly to *PRR5*, with delayed expression in the *prr7;prr9* double mutant owing to longer expression of LHY and CCA1 under LD and LL but not DD, and an advanced phase in the *lhy;cca1* double mutant (figure 5*h*,*p*). In contrast to *PRR5* but similarly to *PRR9* and *PRR7*, *GI* was de-repressed from ZT10 in the *elf3* mutant ($p < 0.01$), consistent with [21] and the Southern dataset (electronic supplementary material, figure S5*f*). The Southern dataset showed that the expression of *GI* was similar in *elf3* and *elf4* mutants, but there was much less effect on *CCA1* in *elf4* than *elf3* (electronic supplementary material, figure S5*g*), indicating that the effects of the EC components can be distinct.

2.5.5. *ELF3*

The *ELF3* rhythmic profile has low amplitude, as noted above, with a trough at ZT2–4 and peaks at both ZT8 and ZT18–20 in WT plants under LD in the TiMet and ROBuST datasets (figure 5*i*,*s*; electronic supplementary material, figures S3*i*–*j*, S5*d*). The trough of ELF3 expression is de-repressed at ZT4 in the *lhy;cca1* double mutant ($p < 0.01$), though there is no peak at this time, in contrast to all the other clock genes. The rise in *ELF3* expression is delayed in the *prr7;prr9* double mutant ($p < 0.01$–0.05, at ZT6–10), consistent with repression by increased levels of LHY and CCA1 (figure 5*i*). The *elf3–4* allele contains a small deletion in the coding region [50] and accumulates the mutant RNA. The mutant expression profile suggests de-repression at ZT2 ($p = 0.06$; figure 6*i*), consistent with lower expression of *LHY* and *CCA1* in *elf3* (noted above).

2.5.6. *ELF4* and *LUX*

The two remaining EC components tested, *ELF4* and *LUX*, share the evening expression peak determined by *LHY*/*CCA1*-mediated repression, with a phase advance in *lhy;cca1* and a delay in *prr7;prr9* in LD and LL conditions (figure 5*g*,*j*). Strikingly, however, the phase separation among the clock genes was lost in the *lhy;cca1* double mutant under LL, such that *PRR9* and *ELF4* peaked together at 50 and 66 h (discussed below). Thus, LHY and CCA1 contribute to the 4 h separation of peak times between *PRR9* (54 h) and *ELF4* (58 h) in the Ws-2 control under LL. In DD, peak expression of *ELF4* was the most reduced of all the genes, to less than 10% of the LD peak level ($p < 0.01$ in Col and Ws; figure 5*t*), consistent with the loss of light activation [44] and/or sugar signalling. *ELF4* was also de-repressed earlier in the *toc1* mutant under DD than the other genes (ZT28–36 h; figure 5*j*), rising as early as in the *lhy;cca1* double mutant. Under LD conditions, the *toc1* mutant de-repressed *ELF4* at ZT2–6, earlier than WT. Peak expression of *LUX* did not fall significantly in DD (figure 5*q*).

LUX was broadly de-repressed in the *elf3* mutant, remaining at the WT peak level at ZT6–22 h (figure 6*g*), in a similar pattern to *PRR7*. This result is consistent with LUX binding to its cognate promoter [20] resulting in negative autoregulation (figure 1*a* [10]). *ELF4* expression in the *elf3* mutant, in contrast, showed a pattern more similar to *TOC1* and *PRR5* (see above), with de-repression only from ZT22–ZT6 h (figure 6*j*).

2.6. Alternative visualization gives new insights into co-regulation of clock genes

Data visualization is critical in analysing the complex interactions within the clock gene circuit, in order to generate new hypotheses. Timeseries plots do not show these interactions directly. They can be revealed in phase plane diagrams that plot the levels of two components against each other (figure 7), though this format is less familiar (see electronic supplementary material). First, phase plane plots emphasize the relative timing of clock components, rather than control by the light : dark cycle. For example, *GI* rose without (before) *TOC1*, especially in Col plants of the TiMet and ROBuST datasets that were grown without exogenous sucrose. High *TOC1* levels extended later than high *GI*, particularly in Ws-2 plants of the TiMet datasets (figure 7*a*). Second, this visualization can reveal interactions among the components plotted. For example, figure 7*b* shows *TOC1* RNA levels in younger plants were maintained at 35–55% of the peak level at ZT20–22, when *CCA1* expression rose above 50% of its peak level. *TOC1* levels were lower for the same *CCA1* level in rosette plants. The logarithmic scale shows this more clearly (figure 7*c*). This suggests that CCA1 protein is not yet an effective repressor of *TOC1* at this phase, especially in younger tissues.

Finally, the phase plane diagrams can show how the interaction of two genes depends upon a third regulator. Expression peaks of *PRR9* and *ELF4* were far out of phase in the WT (figure 7*d*), for example. Data from LL (filled symbols) suggest a negative correlation in the subjective night, when *ELF4* falls as *PRR9* rises. However, the two genes peak then fall together in the *lhy cca1* double mutant under LL, at ZT26 and ZT42 (figure 7*e*; equivalent to timepoints 50 and 66 h in figure 5), creating a diagonal with a positive gradient (red dashed line, figure 7*f*). *PRR9* also had an earlier peak that was not shared by *ELF4* (ZT22 and ZT38, or 46 and 62 h in figure 5; black arrowheads in figure 7*f*). Both features were reproduced on two successive cycles, though *PRR9* expression was less than 1% of the WT peak level. Thus *LHY*, *CCA1* and the LD cycle all differentiate *PRR9* expression from *ELF4*, but in their absence, *PRR9* and *ELF4* expression profiles are similar for much of the circadian cycle (six of eight timepoints in the short, 16 h cycle of the mutant), presumably controlled by the other PRRs and/or the EC. Likewise, phase plane diagrams for the *prr7;prr9* double mutant (electronic supplementary material, figure S6) suggested that not only CCA1 and LHY, but also the PRRs repress *ELF4* in the WT. In addition to visualization, many other aspects of data management benefit significantly from online data infrastructure.

2.7. Online infrastructure for data sharing

Our open-source BioDare (Biological Data repository) [51] supports data from many small-scale experiments that collectively represent a significant resource (table 1). Empirical evidence indicates that these data are essential to understand complex biological regulation, and mathematical analysis shows why

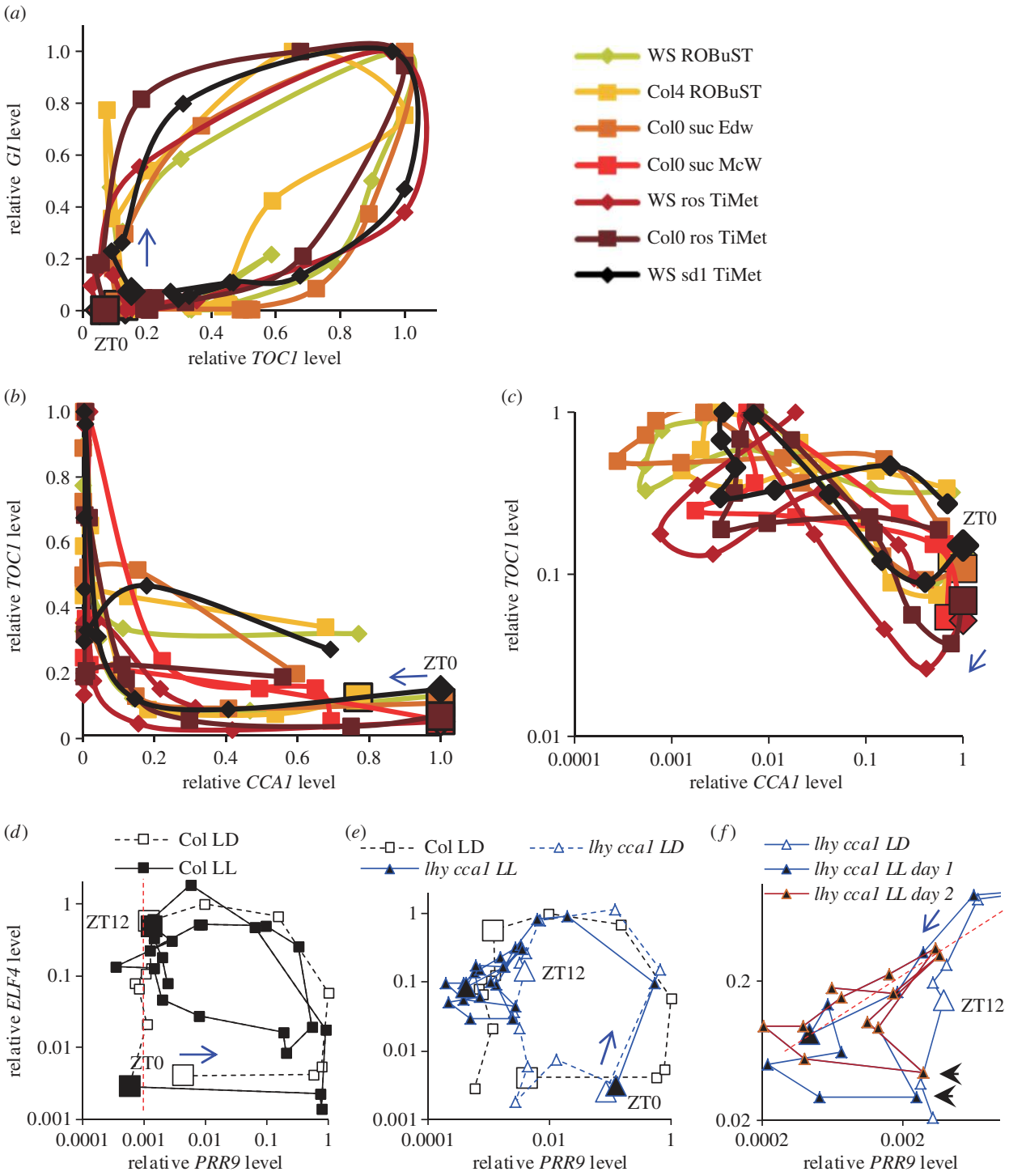

Figure 7. Phase plane diagrams reveal pairwise gene interactions. (*a–c*) Normalized RNA profiles of figure 3 are represented as phase plane diagrams, plotting (*a*) *GI* and *TOC1*, and *TOC1* and *CCA1* on (*b*) linear and (*c*) logarithmic scales. Larger markers indicate ZT0 datapoint, arrows indicate the direction of time. (*d–f*) RNA profiles of figure 5 are represented as phase plane diagrams on logarithmic scales, plotting data for *ELF4* and *PRR9* (*d*) in wild-type Col plants under LD and LL (0–22 h in figure 5, dashed line; 24–70 h, solid line), and (*e*) in Col plants under LD and *lhy cca1* double mutants under LD and LL (solid blue line), with (*f*) a rescaled view of a subset of the data from the *lhy cca1* double mutants. Larger markers indicate 0 (ZT0) and 12 h (ZT12) datapoints in the cycle labelled LD. These timepoints are equivalent to 24 (ZT0) and 36 h (ZT12) in the cycle labelled LL. Arrows indicate the direction of time. (*d*) Red dashed line marks falling *ELF4* levels during the night-time trough of *PRR9* in LD. (*f*) Red dashed line marks correlated *PRR9* and *ELF4* levels; arrowheads mark an earlier peak on each cycle in *PRR9*. Timepoints 48 (ZT24) to 70 h (ZT46) under LL are plotted in brown to emphasize the similar profiles on successive days.

this is the case (see Discussion). In addition to six rhythm-analysis algorithms [52] and protocols for analysis, statistical summary and visualization [53], BioDare facilitates data sharing and public dissemination by providing a stable identifier for each experiment. Detailed metadata (experimental description) ensure that the data can be reused appropriately. Results can be compared across studies and laboratories ('data aggregation') by searching the metadata for genotype, marker gene and other terms (figure 8). Increased expression of *GI* in the *elf3* mutant, for example, is highlighted despite the greater technical variability of manual assay preparation in the Southern dataset compared with the later, robotized assays in the TiMet data (figure 6*h*; electronic supplementary material, figure S5*f* and Methods).

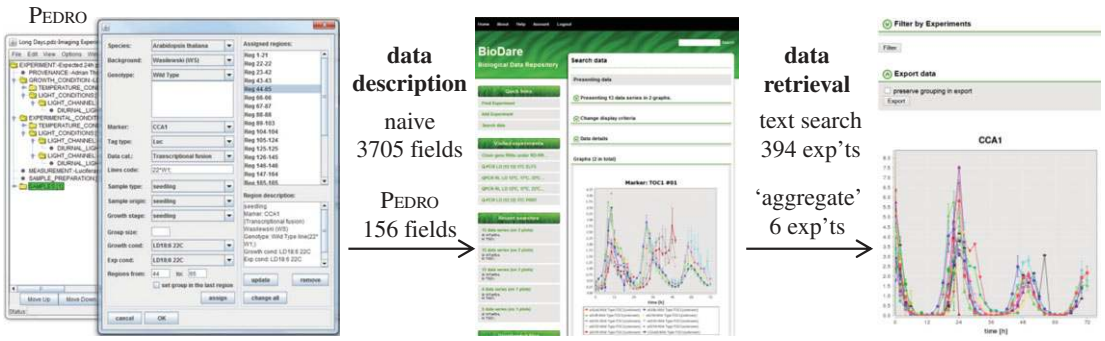

Figure 8. Computational infrastructure for systems chronobiology. Customized wizards in the PEDRO XML editor capture detailed metadata (right panel, showing *CCA1 : LUC* in sample wizard). Rather than filling 3705 metadata fields for this experiment, as a naive spreadsheet would require, PEDRO captures the information with only 156 entries. After uploading the metadata and numerical data to BioDare, results can be displayed in the web browser (centre panel) with powerful secondary processing functions. The left-hand sidebar in this screen has shortcuts to common tasks and recent activity. A naive text search for 'CCA1' returned 394 experiments (exp'ts), whereas BioDare's 'aggregate' function retrieved six specific results by searching the structured metadata, with secondary filters. The search shown (right panel) aggregated qPCR assays of *CCA1* in wild-type plants (see main text) including datasets 1, 3, 4 and 6 of figure 1*c*. The export button above the graph downloads the data shown to a spreadsheet-compatible file.

Table 1. Usage statistics of BioDare (Feb 2015), from originating groups and selected external users. An experiment represents a dataset similar to one of the above-described studies, which includes multiple timeseries, from samples of multiple genotypes, assays or reporters and/or environmental conditions. Totals include minor users that are not listed individually; the total number of data points is over 41 million.

research group	location	experiments	% total experiments	timeseries	% total timeseries
A. J. Millar	Edinburgh, UK	332	14	41 890	18
A. Hall	Liverpool, UK	261	11	79 228	34
D. Bell-Pedersen	Texas A&M, USA	138	6	1428	1
J. Agren	Uppsala, Sweden	18	1	9370	4
K .J. Halliday	Edinburgh, UK	230	10	5043	2
L. Larrondo	Santiago, Chile	75	3	6429	3
M. Jones	Essex, UK	89	4	3148	1
M. Hastings	MRC LMB, UK	1071	45	58 770	25
S. Harmer	UC Davis, USA	37	2	11 353	5
S. A. Kay	USC, USA	38	2	12 972	6
All BioDare		2344		232 844	

2.8. Optimizing clock models with public resources

One goal of such comparisons is to determine how much of the available data is matched by a particular mathematical model: the ROBuST and TiMet experiments were designed to test models of the clock gene circuit under different growth conditions. However, testing complex models against large datasets requires skills that are rare among plant molecular researchers. We therefore tested whether our comprehensive data and better computational resources could make modelling more accessible. The open-source SBSI allows non-programmers to optimize model parameters in order to match diverse data, on large, parallel computers [29]. As a test case, we addressed a recognized limitation of the original P2011 model [10], termed P2011.1.1. The model was developed to understand circadian clock function under light–dark cycles and, separately, under constant light. Following a transition from LD to LL (as in figure 5*a–j*), the first peak in expression of the combined *LHY/CCA1* component under constant light occurred at ZT28.4 h (52.4 h in figure 7*a*), about 2.5 h later than in the TiMet ros data (as noted [25,54]). The model's light–dark function was replaced with the input signal step function [55] to represent the LD–LL transition in the community model exchange format, SBML [56]. The resulting model P2011.1.2 was optimized in SBSI (see electronic supplementary material), testing model simulations with many alternative parameter sets against the TiMet ros RNA dataset, including the LD–LL transition (figure 5*a–j*), and against circadian period values for clock mutants and WT plants [29].

The optimized parameter set of model P2011.2.1 more closely matched the data, including an earlier peak of *LHY/CCA1* in LL at ZT26.5 h (figure 9*a*) and a closer match to *TOC1* and *GI* profiles in LD (ZT10–12 h; figure 9*b,c*), while retaining other qualitative behaviours. *LHY/CCA1* expression rises in LL after the PRR repressor proteins are degraded. Consistent with this notion, removing *TOC1*, the last gene in the *PRR* repressor wave, advanced the phase of the entire clock mechanism in LL. Results for *PRR7* are shown in figure 9*d,e*. PRR protein degradation rates were not strongly affected in P2011.2.1; rather, overall PRR levels were lower than in P2011.1.2 (not shown). In the simulated *toc1* mutant, the peak of *LHY/CCA1* was 1.4 h earlier than simulated WT in P2011.1.2, 2.5 h earlier in P2011.2.1, but 4 h earlier in the data (figure 5*a,b*). The simulations of *PRR7* show the same improved timing of the new

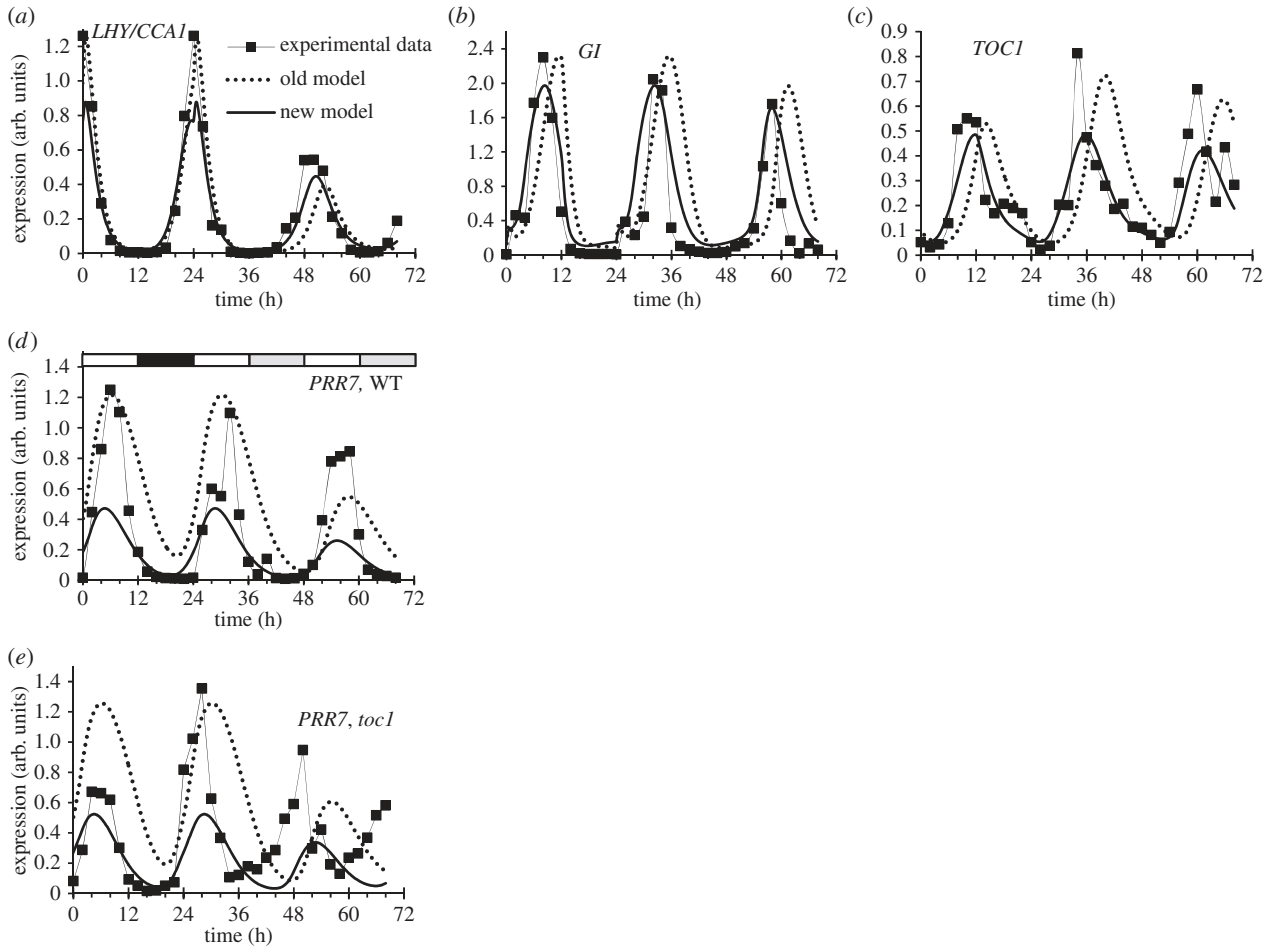

Figure 9. Model re-optimization. Comparison of measured transcript levels from figure 5 (experimental data, symbols), with simulation of models P2011.1.2 (old model, dotted line) and P2011.2.1 (new model, solid line), which resulted from fitting to these data using SBSI. 0–24 h, LD; 24–72 h, LL. (*a*) *LHY* and *CCA1* transcripts are combined in the model, so the average of *LHY* and *CCA1* data is plotted. The peak of *LHY/CCA1* under LL was delayed in the P2011.1.2 model (52.4 h) relative to the peak in the data (50 h), which was closely matched by the P2011.2.1 model (50.5 h). (*b*) *GI* transcript, (*c*) *TOC1* transcript and (*d*) *PRR7* transcript in Col-0 WT. (*e*) *PRR7* transcript in the *toc1* mutant shows a greater phase-advance in LL than either model. Chi-square cost value for match to TiMet ros Col-0 data in LD-LL was 20.2 for P2011.1.2, 7.6 for P2011.2.1. Chi-square cost for match to TiMet ros *toc1* data in LD-LL was 39.7 for P2011.1.2, 13.1 for P2011.2.1.

Table 2. Optimization of model parameters from loose constraints. The starting P2011.1.2 model was optimized in SBSI to fit the TiMet ros dataset and additional period constraints (see electronic supplementary material, Methods). Model, version number of the resulting model. PlaSMo ID, model identifier in the PlaSMo resource. Job, computational job code. Start, the default parameters values from P2011.1.2 or nominal values (Nom). Range, the range of parameter values that were searched, either as fold change above and below the P2011.1.2 values or as a fixed range. Set-up trials, the number of randomly chosen parameter sets tested to initialize the optimization. Cost, the best cost value (closest fit to all constraints).

model	PlaSMo ID	internal job ID	start	range	set-up trials	cost
P2011.1.2	PLM_71 ver 1	—	—	—	—	171
P2011.2.1	PLM_71 ver 2	.599	P2011.1.2	2–3×	5000	77
P2011.3.1	PLM_1041 ver 1	t30	P2011.1.2	100×	2 097 152	175
P2011.4.1	PLM_1042 ver 1	t34	Nom	0.001–10	67 108 864	270
P2011.5.1	PLM_1043 ver 1	t37	Nom	0.001–10	67 108 864	190
P2011.6.1	PLM_1044 ver 1	t40	Nom	0.0005–20	134 217 728	185

model for the WT (figure 9*d*) and the *toc1* mutant in LD (figure 9*e*), but an earlier phase of the *toc1* mutant data under LL. Regulatory interactions among the *PRR* genes will repay further analysis [9,10] in future models (see Discussion).

The computation time required for P2011.2.1 was only approximately 30 core-hours, because the model parameters were varied within only a narrow range (two- to threefold change) from their starting values in P2011.1.2 [10]. The P2011.1.2 parameters had been manually determined to match a wide range of data and qualitative behaviours in the clock literature; many were derived from the parent model P2010 [14]. When the first model of a system is developed, in contrast, most or all parameter values may be unknown. We therefore tested our approach in such scenarios (table 2). Allowing parameter values to differ by up to 100-fold from the values in P2011.1.2 created a very large parameter space

that was nonetheless centred on a known, viable region. In contrast, starting parameters from nominal values (0.1, 1, etc.) and testing each parameter over the same range (such as 0.001–10) removed that anchor. Viable parameter sets that gave cost values similar to the unmodified P2011.2.1 were identified in each test, with computation times up to four core years for P2011.6.1, using the UK national supercomputing resource HECToR. These parameter sets are not intended to replace P2011.1.2 but to demonstrate that similar results can be achieved by a more accessible approach using the TiMet data and SBSI, without new programming or laborious, manual model development. The P2011 model versions and the cognate graphical network diagram (electronic supplementary material, figure S2) are publicly accessible from the PlaSMo repository and elsewhere (see appendix A).

3. Discussion

3.1. Robust regulation of clock gene expression

Quantitative timeseries data are crucial to understand the dynamics of any moderately complex regulatory system. As understanding advances, more precise questions can be formulated that demand both consistent and comprehensive datasets. We provide such data for the RNA profiles of genes associated with the *Arabidopsis* circadian clock, with an online resource to facilitate comparisons within and across datasets. Our experiments were designed to test clock function under the distinct conditions required for separate studies, on light signalling (in the ROBuST project) and carbon metabolism (in the TiMet project), using different technical platforms. The results presumably include the variation previously observed among experiments designed to be replicated across laboratories [57]. We compared two *Arabidopsis* accessions. Significant differences in circadian timing have been demonstrated among *Arabidopsis* accessions, albeit using long-term, imaging assays that integrate the effects of small timing changes over many cycles [58–60]. Importantly, the rhythmic RNA profiles tested here were remarkably consistent (figure 3). Progress in understanding the clock gene network must, in part, be attributed to this robustness of circadian regulation.

Several clock genes are regulated with high daily amplitude, more than 100-fold for *LHY, CCA1, GI, ELF4* and *PRR5* under LD (figure 4; electronic supplementary material, figures S3 and S4 [21,34]), falling to low RNA copy numbers per cell. Our data necessarily reflect the mean expression across cells in the rosette, greater than 80% of which are in the leaf mesophyll [61]. Nonetheless, the absolute calibration of our RNA assays provides one approach for future estimation of the average copy number for the cognate proteins.

The most striking variations of RNA profiles among WT plants involved the acutely light-responsive genes *GI* and *PRR9*. The ROBuST dataset showed the highest levels of *GI* and strong induction of *PRR9* at ZT2 (figures 2 and 3). This is consistent with strong light induction, which might be mediated by direct photoreceptor signalling and/or by indirect sugar signalling. The absence of exogenous sucrose in the ROBuST conditions was not the sole cause, as the TiMet sd2 data used the same, sucrose-free media but did not show such strong *GI* induction (figure 3*c*). The lower growth temperature in ROBuST conditions (17°C rather than 20–22°C in other datasets) might also increase light responsiveness. Consistent with this notion, both exogenous sucrose and higher ambient temperature limit other light responses [30,31].

3.2. Regulation of the *PRR* repressors

RNA profiles of the *PRR* gene family varied among datasets in the WT under LD, as well as among conditions and genotypes. The variable expression of *TOC1* around ZT18 (figure 3*b*) awaits a mechanistic explanation, as do the de-repression of multiple genes in DD (for example, figure 5*n*) and of *PRR5* in the *gi* mutant (figure 5*e*; electronic supplementary material, figure S5*b*). TOC1 is thought to be an active repressor at ZT18, so variable auto-repression is possible and might also explain variation in *PRR5* expression at this phase (figure 2*g*). Alternatively, *TOC1* expression might rise during a transition between one repressor in the early night (such as the EC) and another in the late night (such as LHY and CCA1).

The tight interconnections among the clock components complicate the analysis of these data, though the resulting combination of direct and indirect effects is now interpretable. For example, removing EC regulation in the *elf3* mutant de-repressed the direct EC targets *PRR9* and *PRR7* in the early night, when the EC is active in WT plants. *PRR5* and *TOC1* were noted as potential targets based on mutant RNA profiles [10], but both genes were de-repressed around dawn in *elf3*, suggesting that an indirect mechanism owing to lower LHY and CCA1 levels is more significant than the loss of direct regulation by the EC in the mutant. *PRR9* and *PRR7* are both proposed EC targets (along with *ELF4* and *LUX*), yet *PRR9* (and *ELF4*) retains rhythmic regulation in the *elf3* mutant under LD, whereas *PRR7* (and *LUX*) is more severely affected (figure 6). To understand such differences in response, it will now be important to measure the affinity of regulators for their target genes, extending initial data [62]. Previous modelling results indicated that the different daily profiles of the *PRR* genes allow flexible responses to dawn and dusk [14], so the mechanisms that generate the *PRR* profiles will repay further analysis [10,11].

Several results suggested that regulation by the *PRR* genes is light-dependent. First, in the *prr7;prr9* double mutant, *LHY* and *CCA1* expression was de-repressed during the day but returned to match the WT profile at night in LD (figure 5). One explanation might be that PRR9 and PRR7 (directly or indirectly) antagonize the light activation of *LHY* and *CCA1* during the day in the WT [14,63], and the absence of these PRR proteins in the double mutant has little effect in darkness. Consistent with this notion, the *prr9* single mutant also showed a day-time de-repression of *CCA1* in the ROBuST dataset (electronic supplementary material, figure S5*e*), albeit less than in the double mutant. However, the *CCA1* profile in the *prr7* single mutant was unaffected in the daytime, but de-repressed 2 h earlier in the night (electronic supplementary material, figure S5*e*). Thus, inter-regulation of the early *PRR* genes is important, in addition to regulation by *TOC1* [10]. Second, in the *lhy;cca1* double mutant, *PRR* gene expression is repressed to low levels at the end of the day in LD, consistent with simultaneous, early expression of all the PRR repressors in these mutant plants. In DD, however, the falling phase of *PRR* expression is the same in WT and double mutant plants (figure 5). The higher and earlier expression of the *PRR* RNAs in the double mutant in DD does not appear to be effective in

suppressing *PRR* expression. The faster degradation of the PRR proteins in darkness presumably contributes to these effects; it will be interesting to determine whether the interaction of the photoreceptor PHYB with clock proteins (including TOC1 [64]) also mediates the light sensitivity of this process.

3.3. Effects of exogenous sucrose

Current models of the *Arabidopsis* circadian clock are necessarily based on disparate data, much of it derived from seedlings grown on media containing high levels of sucrose. The presence or absence of exogenous sucrose under the conditions tested here affected the clock RNA profiles less, or at least no more, than other experimental parameters, despite the widespread regulation of plant genes by sucrose [41,65]. Consistent with this, effects of exogenous sucrose on clock gene expression in WT plants have previously been reported under very low light fluence rates or in the presence of photosynthetic inhibitors [40], in DD, CO_2-free air or the starchless *pgm* mutant [39,66,67]. *PRR7* was induced in sugar-starved conditions (extended DD and at night in *pgm*) and was repressed by resupply of 3% exogenous sucrose (electronic supplementary material, figure S7*a*). Only the TiMet rosette study tested *PRR7* in DD, finding increased *PRR7* levels (figure 5*n*), especially in the trough of the profile (electronic supplementary material, figure S4*c*). Trough levels of *CCA1* and *GI* were also raised in DD in the TiMet data, and in the Edwards experiment that included 3% exogenous sucrose (electronic supplementary material, figure S3 [34]). De-repression of the trough levels in DD is neither specific to *PRR7* nor to sugar limitation. Transcript levels of the TOC1- and PRR5-degrading F-box protein ZTL, and its homologues LKP2 and FKF1, also rose slightly in sugar-starved conditions (electronic supplementary material, figure S7*b* [67]), suggesting one possible mechanism for de-repression of *PRR7* via faster degradation of PRR repressors.

3.4. Open resources for small-scale results

Our results will be useful to generate and test many hypotheses beyond those reported here. The potential for such future value might, in principle, justify the additional effort in curating and disseminating our data. In practice, future value motivated little data sharing, compared with present value. We therefore outline the mathematical understanding of and empirical evidence for such present value, together with practical steps that increased both present and future value relative to the effort involved in sharing data.

No suitable community repository existed for our results. One reason was the relatively large effort required to describe accurately many small data files, which deters researchers and resource developers from sharing such data [68]. The largest-scale omics and sequencing studies have different data structures, motivations, stakeholders and economics, which can facilitate data sharing [69] including exemplary resources in the circadian field [70–72]. However, mathematical analysis explains why the results of small-scale experiments are often particularly valuable in understanding biological systems. Gutenkunst *et al.* [73] showed that parameters were 'sloppy' in dynamic models of a range of biological regulatory systems, meaning that a wide range of parameter values could generate the simple behaviours that they tested. Rand *et al.* [74–76] tested how many parameter changes could affect the dynamic behaviour of such systems. All possible behaviours were tested and only a handful of behaviours could be readily achieved by changing parameters (these behaviours have also been termed the 'dynatype' of the system, by analogy to the phenotype of an organism [77]). For circadian clocks, a change in period was the most accessible behaviour: many different parameter changes altered period under constant conditions [74]. The related, empirical result is that genetic screens seeking mutants with altered circadian period have not only identified clock components, but also many genes that affect the clock less directly [78,79]. Observing a change in period gives little evidence for the role of the mutated gene in the plant and does not strongly constrain any particular parameter in the model, but rather has a small constraining effect upon a large number of parameters, in agreement with Gutenkunst *et al.* [73]. A measured period value can therefore easily be accommodated without fundamentally changing the model. In contrast, manipulating the system to test less accessible behaviours provides strong constraints, albeit potentially on fewer parameters [76]. It is much more likely that such results would not be accommodated by any reasonable parameter values, falsifying the current model and leading to new understanding during the development of a better model. Thus, the number of manipulations tested is crucial; model analysis can prioritize the most informative manipulations [80,81].

One consequence for experimental design is that the number of manipulations is more important than the number of components tested. This concept is familiar from the statistical clustering of microarray timeseries. The behaviour of a single cluster mean can adequately represent hundreds of individual transcripts, even for genes with complex light and circadian regulation [82]. The individual transcript data are more valuable in identifying coregulated, downstream genes than in understanding the clock system upstream. Thus, targeted qRT-PCR or reporter gene assays have been more widely used in understanding the clock gene circuit, although they lacked a data-sharing resource. Despite the limited justification for costly omic assays, targeted data-sharing resources [67,70] have ensured that a subset of transcriptomics data have been reused effectively in clock studies.

Empirical evidence for the value of multiple manipulations comes from 10 years of modelling the plant clock gene circuit and output pathways. Constraining the models with timeseries data from many conditions was a critical tool [83], resulting in multiple, experimentally validated predictions. Gleaning the data from electronic supplementary material or by 'scraping' numerical values from published charts made this possible. In practice, aggregating the numerical data has often taken a major effort, after which the data were shared on author web sites [25,84] or on BioDare [82,85,86].

BioDare [51] was developed to share timeseries data from relatively small-scale experiments conducted within individual laboratories (such as the Edwards, Southern and McWatters datasets) or in collaborative projects with few partners (such as ROBuST and TiMet). A regular user might upload an experiment with several hundred timeseries each week [87,88]. However, the user must also provide experimental metadata that are sufficiently detailed to pinpoint the most relevant experiment among hundreds to thousands of similar studies (table 1). The resource must therefore streamline the process of writing the structured metadata to minimize the weekly effort involved, and then use the metadata to provide

powerful search functions, for later users to discover relevant data that were previously unknown to them. Figure 8 illustrates metadata capture using 'wizard' forms in BioDare, data aggregation based upon the resulting metadata, and visualization of the data from a small set of relevant experiments, whereas a naive text search returned an impractically large number of results.

The potential future value of shared data resulted in fewer than a dozen datasets being shared in the early phases of our projects. To provide immediate value from depositing data, BioDare therefore offers data processing (detrending, averaging) and visualization along with specialized circadian data analysis [52,53]. Stable identifier URLs conveniently direct collaborators to specific datasets and can be cited in publications [88,89]. The citations will be tracked by the Thomson Reuters Data Citation Index, giving a metric analogous to publication citations to recognize data-sharing contributions [90]. BioDare is available as a community resource that could be linked to organism-specific databases [91]. BioDare complements our repository of plant systems models (PlaSMo) [92].

3.5. From visualization to modelling

Our analysis here was model-assisted but manual, so data visualization was important. For example, phase-plane diagrams can reveal conditional pairwise interactions including subtle effects at low RNA levels, such as the correlation of *PRR9* and *ELF4* expression in the *lhy cca1* double mutant under LL (figure 6*d–f*). In contrast, *PRR9* and *ELF4* expression are uncorrelated or anticorrelated in the WT under LD. Such changes in dynamics are important in forming hypotheses during model development. Expert modelling has a subjective element. Objective machine-learning methods can also to contribute to hypothesis generation [93], though understanding such a conditionally connected network (electronic supplementary material, figure S2) is challenging by any approach [94].

Dense transcriptional regulatory interactions might be general for plant environmental response pathways [95], justifying investment in infrastructure to support their analysis. Mathematical models can powerfully express hypotheses about such circuits, so long as the starting model adequately recapitulates most data. Qualitatively, the variation among our datasets was smaller than the departure of the model simulations from the data (figures 3 and 9). The existing circadian clock models are therefore equally applicable to the several growth conditions tested, at least in leaf tissue.

The transition from LD to LL is one case where the model departed from the data, to which it had not previously been constrained (also noted in references [54,88]). The P2011.2.1 model's 2 h late phase in LL (figure 9) is caused by the slower degradation of PRR proteins in the light than in the dark [16,45]. Without a dark night to reduce PRR levels, their slow degradation delays the rise in *LHY/CCA1* on the first cycle in LL in the model. *PRR9*, *PRR7* and *PRR5* RNA levels are reduced in the second cycle in LL in both model and data (figures 5*c–e* and 9*e*), restoring an approximately 24 h period in subsequent cycles. It is reassuring but not surprising that re-optimization of the model could better match this behaviour, but the models' detailed behaviour is non-trivial. Reducing the levels of PRR proteins in the new parameter set advanced the phase of the first peak in LL. Simplified models that included only the PRR protein changes also reduced the effect of the PRRs on the period of the clock in constant light (data not shown), contradicting the data. The re-optimization allowed multiple parameter changes to advance the phase of the P2011.2.1 model under LL while retaining the observed effects of PRRs on clock period, such as the short period of the *toc1* mutant (figure 9*e*).

Most significantly, this result was obtained using tools designed to be accessible to biological researchers with no specialist computing or mathematical skills. Development of P2011.2.1 required no new programming, nor the hand-crafted cost functions that were used to optimize previous models [25,83–85], nor the laborious, expert parameter exploration used to construct its parent models [10,14,96]. Our intention was that the scarcity of these skills should no longer present an insuperable barrier, though of course they remain beneficial, not least to keep abreast of relevant method development [80]. To test whether this approach could assist new model development, as well as adjustment of an existing model, we repeated the parameter search within a wide range of values and/or after setting P2011.1.2 model parameters to nominal values. Greater computational power is required when there are fewer constraints on the model's parameter values; however, viable solutions were identified (table 2) and suitable computing resources are increasingly accessible [97]. The approach and infrastructure presented here allow a wider range of biologists to engage with complicated models, which will be essential tools to understand the mechanisms and physiological functions of complex biological networks.

Author contributions. Designed experiments: A.F., R.S., K.S., H.G.M., M.S., A.J.M., K.J.H. Performed experiments: A.F., A.P.F., V.M., M.M.S., H.G.M., K.S., A.J.M. Designed infrastructure: T.Z., A.J.M., K.J.H. Built infrastructure: T.Z., A.H.; Analysed data: D.D.S., A.P., M.M.S., H.G.M., A.J.M., M.S., K.J.H. A.F., H.G.M., M.S. and A.J.M. wrote the paper with input from all authors.

Competing interests. We declare we have no competing interests.

Funding. Supported by awards from UK BBSRC and EPSRC (ROBuST BB/F005237/1 and SynthSys BB/D019621/1) and from the European Commission (FP7 collaborative project TiMet, contract 245143). This work made use of the facilities of HECToR, the UK's national high-performance computing service, which was provided by UoE HPCx Ltd at the University of Edinburgh, Cray Inc. and NAG Ltd, and funded by the Office of Science and Technology through EPSRC's High End Computing Programme.

Acknowledgements. We are grateful to Gavin Steel and Kelly Stewart for expert technical assistance, Martin Beaton and Richard Adams for support of BioDare and SBSI, Uriel Urquiza for preparing SBML files, David Rand for insightful discussion, and members of the A.J.M. and K.J.H. laboratories, who curated data for BioDare.

Appendix A

A.1. Experimental procedures

Experimental methods were similar or identical to published protocols [33,88,98], as detailed in the electronic supplementary material. Statistical significance of comparisons reported in the results is from two-tailed *t*-tests compared with the cognate WT plants at the same timepoint, unless otherwise stated. Homoscedasticity is assumed, because all comparisons reported are within individual datasets for the same PCR primers. Significance is not corrected for multiple comparisons (reducing significance), nor for support from neighbouring timepoints or replication across cycles or studies (which can increase significance).

A.2. Biodare and computational methods

The BioDare online resource (www.biodare.ed.ac.uk) uses a desktop application to prepare metadata (describe experiments). The XML editor Pedro [99] was customized for each experimental protocol to speed up metadata entry, as each experiment can comprise several hundred samples. Numerical data are uploaded in a spreadsheet-compatible format, with the XML metadata, and stored in a relational database. Password-protected access allows controlled data sharing or public dissemination. Searching the metadata (by genotype, marker, etc.) allows aggregation of similar data from multiple sources, followed by secondary processing (detrending, normalization, averaging), visualization (figure 7*a*) and download. Rhythm analysis in BioDare was recently described [52,53]. Model optimization used SBSIvisual v. 1.4.5 [29] and SBSInumerics v. 1.2 (see electronic supplementary material, Methods). Graphical network diagrams used SBGN-ED in VANTED [38].

A.3. Data, network diagram, model and code accessibility

The accessibility of resources used in the publication is summarized at the University of Edinburgh's institutional repository, at http://www.research.ed.ac.uk/portal/en/datasets/data-code-and-models-for-flis-et-al-rs-open-biology-2015(fd297498-7d0d-4d57-9040-769af9c65212).html

A.3.1. RNA expression profile data

The RNA datasets reported here are publicly available from BioDare with the permanent data identifiers listed below, using login name 'public' with password 'public'. Numbers below match figure 1.

(1) Pinas-Fernandez and K.J. Halliday (2015) ROBuST RNA timeseries data at 17°C for clock model parameterisation. BioDare accessions:

ROBuST sd for *CCA1*, BioDare accession 12820611467827, https://www.biodare.ed.ac.uk/robust/ShowExperiment.action?experimentId=12820611467827

ROBuST sd for *LHY*, BioDare accession 3492, https://www.biodare.ed.ac.uk/robust/ShowExperiment.action?experimentId=3492

ROBuST sd for *PRR9*, BioDare accession 12820610743262, https://www.biodare.ed.ac.uk/robust/ShowExperiment.action?experimentId=12820610743262

ROBuST sd for *PRR7*, BioDare accession 12820611319996, https://www.biodare.ed.ac.uk/robust/ShowExperiment.action?experimentId=12820611319996

ROBuST sd for *PRR5*, BioDare accession 12820611188065, https://www.biodare.ed.ac.uk/robust/ShowExperiment.action?experimentId=12820611188065

ROBuST sd for *TOC1*, BioDare accession 12820611587928, https://www.biodare.ed.ac.uk/robust/ShowExperiment.action?experimentId=12820611587928

ROBuST sd for *GI*, BioDare accession 12820606741450, https://www.biodare.ed.ac.uk/robust/ShowExperiment.action?experimentId=12820606741450

ROBuST sd for *LUX*, BioDare accession 12820610913763, https://www.biodare.ed.ac.uk/robust/ShowExperiment.action?experimentId=12820610913763

ROBuST sd for *CAB2*, BioDare accession 13228354371807, https://www.biodare.ed.ac.uk/robust/ShowExperiment.action?experimentId=13228354371807

ROBuST sd for *ELF4*, BioDare accession 12962296599986, https://www.biodare.ed.ac.uk/robust/ShowExperiment.action?experimentId=12962296599986

ROBuST sd for *ELF3*, BioDare accession 12962294335805, https://www.biodare.ed.ac.uk/robust/ShowExperiment.action?experimentId=12962294335805

(2) Flis, V. Mengin, R. Sulpice and M. Stitt (2015) TiMet RNA timeseries data from rosette plants for clock model parameterisation. TiMEt ros, BioDare accession 2841, https://www.biodare.ed.ac.uk/robust/ShowExperiment.action?experimentId=2841

(3) Flis, V. Mengin, R. Sulpice and M. Stitt (2015) TiMet RNA timeseries data from *elf3* mutant plants for clock model parameterisation. TiMet sd1, BioDare accession 2842, https://www.biodare.ed.ac.uk/robust/ShowExperiment.action?experimentId=2842

(4) Flis, V. Mengin, R. Sulpice and M. Stitt (2015) TiMet RNA timeseries data from seedlings for clock model parameterisation. TiMet sd2, BioDare accession 2843, https://www.biodare.ed.ac.uk/robust/ShowExperiment.action?experimentId=2843

(5) H. G. McWatters (2015) Clock RNA timeseries in light and temperature entrainment. McWatters sd, BioDare accession 3488, https://www.biodare.ed.ac.uk/robust/ShowExperiment.action?experimentId=3488

(6) K.D. Edwards and A.J. Millar (2010). Clock RNA timeseries in multiple photoperiods. Edwards sd, BioDare accession 13227622661196, https://www.biodare.ed.ac.uk/robust/ShowExperiment.action?experimentId=13227622661196

(7) M.M. Southern and A.J. Millar (2015). Clock RNA timeseries in wild-type and mutant plants under red light.

Independent biological replicates are presented for this experiment, with the same genotypes and markers tested in replicates (1 + 2) and (3 + 4):

Southern sd replicate 1, Biodare accession 1322829828 8040, https://www.biodare.ed.ac.uk/robust/ShowExperiment.action?experimentId=13228298288040

Southern sd replicate 2, Biodare accession 132276198 71305, https://www.biodare.ed.ac.uk/robust/ShowExperiment.action?experimentId=13227619871305

Southern sd replicate 3, Biodare accession 1322835 7055348, https://www.biodare.ed.ac.uk/robust/ShowExperiment.action?experimentId=13228357055348

Southern sd replicate 4, Biodare accession 13228357 183121, https://www.biodare.ed.ac.uk/robust/ShowExperiment.action?experimentId=13228357183121

A.3.2. Code

BioDare and SBSI are open-source and available from Sourceforge (www.sourceforge.net).

BioDare: Sourceforge project, http://sourceforge.net/projects/biodare/. The online resource is available at www.biodare.ed.ac.uk.

SBSI: Sourceforge project, http://sourceforge.net/projects/sbsi/. Related materials, plugins and tutorials are available at www.sbsi.ed.ac.uk.

A.3.3. Graphical network diagram

The diagram of the *Arabidopsis* clock model (electronic supplementary material, figure S2) is available from the PlaSMo repository (www.plasmo.ed.ac.uk), which handles a variety of XML file formats.

D. D. Seaton and A. J. Millar (2015), Graphical network diagram of the *Arabidopsis* clock model P2011.1 in SBGN PD: PlaSMo accession 1045 version 1, http://www.plasmo.ed.ac.uk/plasmo/models/model.shtml?accession=PLM_1045&version=1

A.3.4. Models

A. Pokhilko *et al*. (2012), *Arabidopsis* clock model P2011.1.1 (published in Molecular Systems Biology, 2012): BioModels identifier BIOMD0000000412 [100].

The *Arabidopsis* clock models below are available from the PlaSMo repository (www.plasmo.ed.ac.uk) and will also be submitted to Biomodels when the present publication has a digital identifier. The model versioning convention is described in the electronic supplementary material.

A. J. Millar and A. Hume (2015) *Arabidopsis* clock model P2011.1.2: PlaSMo accession PLM_71 version 1, http://www.plasmo.ed.ac.uk/plasmo/models/model.shtml?accession=PLM_71&version=1

A. J. Millar and A. Hume (2015) *Arabidopsis* clock model P2011.2.1: PlaSMo accession PLM_71 version 2, http://www.plasmo.ed.ac.uk/plasmo/models/model.shtml?accession=PLM_71&version=2

K. Stratford, A. Hume and A. J. Millar (2015) *Arabidopsis* clock model P2011.3.1: PlaSMo accession PLM_1041 version 1, http://www.plasmo.ed.ac.uk/plasmo/models/model.shtml?accession=PLM_1041&version=1

K. Stratford, A. Hume and A. J. Millar (2015) *Arabidopsis* clock model P2011.4.1: PlaSMo accession PLM_1042 version 1, http://www.plasmo.ed.ac.uk/plasmo/models/model.shtml?accession=PLM_1042&version=1

K. Stratford, A. Hume and A. J. Millar (2015) *Arabidopsis* clock model P2011.5.1: PlaSMo accession PLM_1043 version 1, http://www.plasmo.ed.ac.uk/plasmo/models/model.shtml?accession=PLM_1043&version=1

K. Stratford, A. Hume and A. J. Millar (2015) *Arabidopsis* clock model P2011.6.1: PlaSMo accession PLM_1044 version 1, http://www.plasmo.ed.ac.uk/plasmo/models/model.shtml?accession=PLM_1044&version=1

References

1. Zhang EE, Kay SA. 2010 Clocks not winding down: unravelling circadian networks. *Nat. Rev. Mol. Cell Biol.* **11**, 764–776. (doi:10.1038/nrm2995)
2. Dong G, Golden SS. 2008 How a cyanobacterium tells time. *Curr. Opin. Microbiol.* **11**, 541–546. (doi:10.1016/j.mib.2008.10.003)
3. Dodd AN *et al.* 2008 Plant circadian clocks increase photosynthesis, growth, survival, and competitive advantage. *Science* **309**, 630–633. (doi:10.1126/science.1115581)
4. Ouyang Y, Andersson CR, Kondo T, Golden SS, Johnson CH. 1998 Resonating circadian clocks enhance fitness in cyanobacteria. *Proc. Natl Acad. Sci. USA* **95**, 8660–8664. (doi:10.1073/pnas.95.15.8660)
5. Kinmonth-Schultz HA, Golembeski GS, Imaizumi T. 2013 Circadian clock-regulated physiological outputs: dynamic responses in nature. *Semin. Cell Dev. Biol.* **24**, 407–413. (doi:10.1016/j.semcdb.2013.02.006)
6. Young MW, Kay SA. 2001 Time zones: a comparative genetics of circadian clocks. *Nat. Rev. Genet.* **2**, 702–715. (doi:10.1038/35088576)
7. van Ooijen G, Millar AJ. 2012 Non-transcriptional oscillators in circadian timekeeping. *Trends Biochem. Sci.* **37**, 484–492. (doi:10.1016/j.tibs.2012.07.006)
8. Le Novere N *et al.* 2009 The systems biology graphical notation. *Nat. Biotechnol.* **27**, 735–741. (doi:10.1038/nbt.1558)
9. Pokhilko A, Mas P, Millar AJ. 2013 Modelling the widespread effects of TOC1 signalling on the plant circadian clock and its outputs. *BMC Syst. Biol.* **7**, 23. (doi:10.1186/1752-0509-7-23)
10. Pokhilko A, Fernandez AP, Edwards KD, Southern MM, Halliday KJ, Millar AJ. 2012 The clock gene circuit in *Arabidopsis* includes a repressilator with additional feedback loops. *Mol. Syst. Biol.* **8**, 574. (doi:10.1038/msb.2012.6)
11. Nakamichi N. 2011 Molecular mechanisms underlying the *Arabidopsis* circadian clock. *Plant Cell Physiol.* **52**, 1709–1718. (doi:10.1093/pcp/pcr118)
12. Farre EM, Harmer SL, Harmon FG, Yanovsky MJ, Kay SA. 2005 Overlapping and distinct roles of PRR7 and PRR9 in the *Arabidopsis* circadian clock. *Curr. Biol.* **15**, 47–54. (doi:10.1016/j.cub.2004.12.067)
13. Salome PA, McClung CR. 2005 PSEUDO-RESPONSE REGULATOR 7 and 9 are partially redundant genes essential for the temperature responsiveness of the *Arabidopsis* circadian clock. *Plant Cell* **17**, 791–803. (doi:10.1105/tpc.104.029504)
14. Pokhilko A, Hodge SK, Stratford K, Knox K, Edwards KD, Thomson AW, Mizuno T, Millar AJ. 2010 Data assimilation constrains new connections and components in a complex, eukaryotic circadian clock model. *Mol. Syst. Biol.* **6**, 416. (doi:10.1038/msb.2010.69)
15. Nakamichi N, Kiba T, Kamioka M, Suzuki T, Yamashino T, Higashiyama T, Sakakibara H, Mizuno T. 2012 Transcriptional repressor PRR5 directly regulates clock-output pathways. *Proc. Natl Acad. Sci. USA* **109**, 17 123–17 128. (doi:10.1073/pnas.1205156109)
16. Nakamichi N, Kiba T, Henriques R, Mizuno T, Chua NH, Sakakibara H. 2010 PSEUDO-RESPONSE REGULATORS 9, 7, and 5 are transcriptional repressors in the *Arabidopsis* circadian clock. *Plant Cell* **22**, 594–605. (doi:10.1105/tpc.109.072892)
17. Huang W, Perez-Garcia P, Pokhilko A, Millar AJ, Antoshechkin I, Riechmann JL, Mas P. 2012 Mapping the core of the *Arabidopsis* circadian clock defines the network structure of the oscillator. *Science* **336**, 75–79. (doi:10.1126/science.1219075)
18. Gendron JM, Pruneda-Paz JL, Doherty CJ, Gross AM, Kang SE, Kay SA. 2012 *Arabidopsis* circadian clock protein, TOC1, is a DNA-binding transcription factor. *Proc. Natl Acad. Sci. USA* **109**, 3167–3172. (doi:10.1073/pnas.1200355109)
19. Nusinow DA, Helfer A, Hamilton EE, King JJ, Imaizumi T, Schultz TF, Farré EM, Kay SA. 2011 The ELF4-ELF3-LUX complex links the circadian clock to diurnal control of hypocotyl growth. *Nature* **475**, 398–402. (doi:10.1038/nature10182)
20. Helfer A, Nusinow DA, Chow BY, Gehrke AR, Bulyk ML, Kay SA. 2011 LUX ARRHYTHMO encodes a nighttime repressor of circadian gene expression in the *Arabidopsis* core clock. *Curr. Biol.* **21**, 126–133. (doi:10.1016/j.cub.2010.12.021)
21. Dixon LE, Knox K, Kozma-Bognar L, Southern MM, Pokhilko A, Millar AJ. 2011 Temporal repression of core circadian genes is mediated through EARLY FLOWERING 3 in *Arabidopsis*. *Curr. Biol.* **21**, 120–125. (doi:10.1016/j.cub.2010.12.013)
22. Herrero E *et al.* 2012 EARLY FLOWERING4 recruitment of EARLY FLOWERING3 in the nucleus sustains the *Arabidopsis* circadian clock. *Plant Cell* **24**, 428–443. (doi:10.1105/tpc.111.093807)

23. Kim WY *et al.* 2007 ZEITLUPE is a circadian photoreceptor stabilized by GIGANTEA in blue light. *Nature* **449**, 356–360. (doi:10.1038/nature06132)
24. Bujdoso N, Davis SJ. 2013 Mathematical modeling of an oscillating gene circuit to unravel the circadian clock network of *Arabidopsis thaliana*. *Front. Plant Sci.* **4**, 3. (doi:10.3389/fpls.2013.00003)
25. Fogelmark K, Troein C. 2014 Rethinking transcriptional activation in the *Arabidopsis* circadian clock. *PLoS Comput. Biol.* **10**, e1003705. (doi:10.1371/journal.pcbi.1003705)
26. The Royal Society. 2012 Science as an open enterprise 2012. 29 June 2012. See https://royalsociety.org/~/media/policy/projects/sape/2012-06-20-saoe.pdf.
27. Hey T, Tansley S, Tolle K (eds). 2009 *The fourth paradigm: data-intensive scientific discovery*. Redmond, WA: Microsoft Research.
28. Bastow R, Leonelli S. 2010 Sustainable digital infrastructure. Although databases and other online resources have become a central tool for biological research, their long-term support and maintenance is far from secure. *EMBO Rep.* **11**, 730–734. (doi:10.1038/embor.2010.145)
29. Adams R *et al.* 2013 SBSI: an extensible distributed software infrastructure for parameter estimation in systems biology. *Bioinformatics* **29**, 664–665. (doi:10.1093/bioinformatics/btt023)
30. Stewart JL, Maloof JN, Nemhauser JL. 2011 PIF genes mediate the effect of sucrose on seedling growth dynamics. *PLoS ONE* **6**, e19894. (doi:10.1371/journal.pone.0019894)
31. Franklin KA, Toledo-Ortiz G, Pyott DE, Halliday KJ. 2014 Interaction of light and temperature signalling. *J. Exp. Bot.* **65**, 2859–2871. (doi:10.1093/jxb/eru059)
32. Salvo-Chirnside E, Kane S, Kerr LE. 2011 Protocol: high throughput silica-based purification of RNA from *Arabidopsis* seedlings in a 96-well format. *Plant Methods* **7**, 40. (doi:10.1186/1746-4811-7-40)
33. Piques M, Schulze WX, Hohne M, Usadel B, Gibon Y, Rohwer J, Stitt M. 2009 Ribosome and transcript copy numbers, polysome occupancy and enzyme dynamics in *Arabidopsis*. *Mol. Syst. Biol.* **5**, 314. (doi:10.1038/msb.2009.68)
34. Edwards KD *et al.* 2010 Quantitative analysis of regulatory flexibility under changing environmental conditions. *Mol. Syst. Biol.* **6**, 424. (doi:10.1038/msb.2010.81)
35. Locke JC, Southern MM, Kozma-Bognar L, Hibberd V, Brown PE, Turner MS, Millar AJ. 2005 Extension of a genetic network model by iterative experimentation and mathematical analysis. *Mol. Syst. Biol.* **1**, 20050013. (doi:10.1038/msb4100018)
36. Strayer C *et al.* 2000 Cloning of the *Arabidopsis* clock gene *TOC1*, an autoregulatory response regulator homolog. *Science* **289**, 768–771. (doi:10.1126/science.289.5480.768)
37. Fowler S *et al.* 1999 GIGANTEA: a circadian clock-controlled gene that regulates photoperiodic flowering in *Arabidopsis* and encodes a protein with several possible membrane-spanning domains. *EMBO J.* **18**, 4679–4688. (doi:10.1093/emboj/18.17.4679)
38. Czauderna T, Klukas C, Schreiber F. 2010 Editing, validating and translating of SBGN maps. *Bioinformatics* **26**, 2340–2341. (doi:10.1093/bioinformatics/btq407)
39. Dalchau N *et al.* 2011 The circadian oscillator gene GIGANTEA mediates a long-term response of the *Arabidopsis* thaliana circadian clock to sucrose. *Proc. Natl Acad. Sci. USA* **108**, 5104–5109. (doi:10.1073/pnas.1015452108)
40. Haydon MJ, Mielczarek O, Robertson FC, Hubbard KE, Webb AA. 2013 Photosynthetic entrainment of the *Arabidopsis thaliana* circadian clock. *Nature* **502**, 689–692. (doi:10.1038/nature12603)
41. Usadel B *et al.* 2005 Extension of the visualization tool MapMan to allow statistical analysis of arrays, display of corresponding genes, and comparison with known responses. *Plant Physiol.* **138**, 1195–1204. (doi:10.1104/pp.105.060459)
42. Osuna D *et al.* 2007 Temporal responses of transcripts, enzyme activities and metabolites after adding sucrose to carbon-deprived *Arabidopsis* seedlings. *Plant J.* **49**, 463–491. (doi:10.1111/j.1365-313X.2006.02979.x)
43. Doyle MR, Davis SJ, Bastow RM, McWatters HG, Kozma-Bognar L, Nagy F, Millar AJ, Amasino RM. 2002 The ELF4 gene controls circadian rhythms and flowering time in *Arabidopsis thaliana*. *Nature* **419**, 74–77. (doi:10.1038/nature00954)
44. Li G *et al.* 2011 Coordinated transcriptional regulation underlying the circadian clock in *Arabidopsis*. *Nat. Cell Biol.* **13**, 616–622. (doi:10.1038/ncb2219)
45. Kiba T, Henriques R, Sakakibara H, Chua NH. 2007 Targeted degradation of PSEUDO-RESPONSE REGULATOR5 by an SCFZTL complex regulates clock function and photomorphogenesis in *Arabidopsis thaliana*. *Plant Cell* **19**, 2516–2530. (doi:10.1105/tpc.107.053033)
46. Yakir E, Hilman D, Hassidim M, Green RM. 2007 CIRCADIAN CLOCK ASSOCIATED1 transcript stability and the entrainment of the circadian clock in *Arabidopsis*. *Plant Physiol.* **145**, 925–932. (doi:10.1104/pp.107.103812)
47. Alabadi D, Oyama T, Yanovsky MJ, Harmon FG, Mas P, Kay SA. 2001 Reciprocal regulation between TOC1 and LHY/CCA1 within the *Arabidopsis* circadian clock. *Science* **293**, 880–883. (doi:10.1126/science.1061320)
48. Millar AJ, Carré IA, Strayer CA, Chua NH, Kay SA. 1995 Circadian clock mutants in *Arabidopsis* identified by luciferase imaging. *Science* **267**, 1161–1163. (doi:10.1126/science.7855595)
49. Carre I, Veflingstad SR. 2013 Emerging design principles in the *Arabidopsis* circadian clock. *Semin. Cell Dev. Biol.* **24**, 393–398. (doi:10.1016/j.semcdb.2013.03.011)
50. Hicks KA, Albertson TM, Wagner DR. 2001 EARLY FLOWERING3 encodes a novel protein that regulates circadian clock function and flowering in *Arabidopsis*. *Plant Cell* **13**, 1281–1292. (doi:10.1105/tpc.13.6.1281)
51. BioDare 2011 The Biological Data Repository. See www.biodare.ed.ac.uk.
52. Zielinski T, Moore AM, Troup E, Halliday KJ, Millar AJ. 2014 Strengths and limitations of period estimation methods for circadian data. *PLoS ONE* **9**, e96462. (doi:10.1371/journal.pone.0096462)
53. Moore A, Zielinski T, Millar AJ. 2014 Online period estimation and determination of rhythmicity in circadian data, using the BioDare data infrastructure. In *Plant circadian networks* (ed. D Staiger), pp. 13–44. Clifton, NJ: Humana Press.
54. Dodd AN, Dalchau N, Gardner MJ, Baek SJ, Webb AA. 2014 The circadian clock has transient plasticity of period and is required for timing of nocturnal processes in *Arabidopsis*. *New Phytol.* **201**, 168–179. (doi:10.1111/nph.12489)
55. Adams RR, Tsorman N, Stratford K, Akman OE, Gilmore S, Juty N, Le Novere N, Millar AJ, Millar AJ. 2012 The Input Signal Step Function (ISSF), a standard method to encode input signals in SBML models with software support, applied to circadian clock models. *J. Biol. Rhythms* **27**, 328–332. (doi:10.1177/0748730412451077)
56. Hucka M *et al.* 2003 The systems biology markup language (SBML): a medium for representation and exchange of biochemical network models. *Bioinformatics* **19**, 524–531. (doi:10.1093/bioinformatics/btg015)
57. Massonnet C *et al.* 2010 Probing the reproducibility of leaf growth and molecular phenotypes: a comparison of three *Arabidopsis* accessions cultivated in ten laboratories. *Plant Physiol.* **152**, 2142–2157. (doi:10.1104/pp.109.148338)
58. Swarup K, Alonso-Blanco C, Lynn JR, Michaels SD, Amasino RM, Koornneef M, Millar AJ. 1999 Natural allelic variation identifies new genes in the *Arabidopsis* circadian system. *Plant J.* **20**, 67–77. (doi:10.1046/j.1365-313X.1999.00577.x)
59. Michael TP *et al.* 2003 Enhanced fitness conferred by naturally occurring variation in the circadian clock. *Science* **302**, 1049–1053. (doi:10.1126/science.1082971)
60. Darrah C, Taylor BL, Edwards KD, Brown PE, Hall A, McWatters HG. 2006 Analysis of phase of LUCIFERASE expression reveals novel circadian quantitative trait loci in *Arabidopsis*. *Plant Physiol.* **140**, 1464–1474. (doi:10.1104/pp.105.074518)
61. Wuyts N, Palauqui JC, Conejero G, Verdeil JL, Granier C, Massonnet C. 2010 High-contrast three-dimensional imaging of the *Arabidopsis* leaf enables the analysis of cell dimensions in the epidermis and mesophyll. *Plant Methods* **6**, 17. (doi:10.1186/1746-4811-6-17)
62. O'Neill JS, van Ooijen G, Le Bihan T, Millar AJ. 2011 Circadian clock parameter measurement: characterization of clock transcription factors using surface plasmon resonance. *J. Biol. Rhythms* **26**, 91–98. (doi:10.1177/0748730410397465)
63. Locke JC, Kozma-Bognar L, Gould PD, Feher B, Kevei E, Nagy F, Turner MS, Hall A, Millar AJ. 2006 Experimental validation of a predicted feedback loop in the multi-oscillator clock of *Arabidopsis*

thaliana. *Mol. Syst. Biol*. **2**, 59. (doi:10.1038/msb4100102)

64. Yeom M, Kim H, Lim J, Shin AY, Hong S, Kim JI, Nam HG. 2014 How do phytochromes transmit the light quality information to the circadian clock in *Arabidopsis*? *Mol. Plant*. **7**, 1701–1704. (doi:10.1093/mp/ssu086)
65. Price J, Laxmi A, St Martin SK, Jang JC. 2004 Global transcription profiling reveals multiple sugar signal transduction mechanisms in *Arabidopsis*. *Plant Cell* **16**, 2128–2150. (doi:10.1105/tpc.104.022616)
66. Blasing OE *et al.* 2005 Sugars and circadian regulation make major contributions to the global regulation of diurnal gene expression in *Arabidopsis*. *Plant Cell* **17**, 3257–3281. (doi:10.1105/tpc.105.035261)
67. Usadel B, Blasing OE, Gibon Y, Retzlaff K, Hohne M, Gunther M, Stitt M. 2008 Global transcript levels respond to small changes of the carbon status during progressive exhaustion of carbohydrates in *Arabidopsis* rosettes. *Plant Physiol*. **146**, 1834–1861. (doi:10.1104/pp.107.115592)
68. Leonelli S, Smirnoff N, Moore J, Cook C, Bastow R. 2013 Making open data work for plant scientists. *J. Exp. Bot*. **64**, 4109–4117. (doi:10.1093/jxb/ert273)
69. Toronto International Data Release Workshop A *et al.* 2009 Prepublication data sharing. *Nature* **461**, 168–170. (doi:10.1038/461168a)
70. Mockler TC, Michael TP, Priest HD, Shen R, Sullivan CM, Givan SA, McEntee C, Kay SA, Chory J. 2007 The DIURNAL project: diurnal and circadian expression profiling, model-based pattern matching, and promoter analysis. *Cold Spring Harb. Symp. Quant. Biol*. **72**, 353–363. (doi:10.1101/sqb.2007.72.006)
71. Zhang EE *et al.* 2009 A genome-wide RNAi screen for modifiers of the circadian clock in human cells. *Cell* **139**, 199–210. (doi:10.1016/j.cell.2009.08.031)
72. Patel VR, Eckel-Mahan K, Sassone-Corsi P, Baldi P. 2012 CircadiOmics: integrating circadian genomics, transcriptomics, proteomics and metabolomics. *Nat. Methods* **9**, 772–773. (doi:10.1038/nmeth.2111)
73. Gutenkunst RN, Waterfall JJ, Casey FP, Brown KS, Myers CR, Sethna JP. 2007 Universally sloppy parameter sensitivities in systems biology models. *PLoS Comput. Biol*. **3**, 1871–1878. (doi:10.1371/journal.pcbi.0030189)
74. Rand DA, Shulgin BV, Salazar D, Millar AJ. 2004 Design principles underlying circadian clocks. *Interface* **1**, 119–130.
75. Rand DA, Shulgin BV, Salazar JD, Millar AJ. 2006 Uncovering the design principles of circadian clocks: mathematical analysis of flexibility and evolutionary goals. *J. Theor. Biol*. **238**, 616–635. (doi:10.1016/j.jtbi.2005.06.026)
76. Rand DA. 2008 Mapping global sensitivity of cellular network dynamics: sensitivity heat maps and a global summation law. *J. R. Soc. Interface* **5**(Suppl. 1), S59–S69. (doi:10.1098/rsif.2008.0084.focus)
77. Daniels BC, Chen YJ, Sethna JP, Gutenkunst RN, Myers CR. 2008 Sloppiness, robustness, and evolvability in systems biology. *Curr. Opin. Biotechnol*. **19**, 389–395. (doi:10.1016/j.copbio.2008.06.008)
78. Dunlap JC. 1993 Genetic analysis of circadian clocks. *Annu. Rev. Physiol*. **55**, 683–728.
79. McWatters HG, Devlin PF. 2011 Timing in plants: a rhythmic arrangement. *FEBS Lett*. **585**, 1474–1484. (doi:10.1016/j.febslet.2011.03.051)
80. Transtrum MK, Machta BB, Sethna JP. 2010 Why are nonlinear fits to data so challenging? *Phys. Rev. Lett*. **104**, 060201. (doi:10.1103/PhysRevLett.104.060201)
81. Domijan M, Rand DA. 2015 Using constraints and their value for optimization of large ODE systems. *J. R. Soc. Interface* **12**, 20141303. (doi:10.1098/rsif.2014.1303)
82. Seaton DD *et al.* 2015 Linked circadian outputs control elongation growth and flowering in response to photoperiod and temperature. *Mol. Syst. Biol*. **11**, 776. (doi:10.15252/msb.20145766)
83. Locke JC, Millar AJ, Turner MS. 2005 Modelling genetic networks with noisy and varied experimental data: the circadian clock in *Arabidopsis thaliana*. *J. Theor. Biol*. **234**, 383–393. (doi:10.1016/j.jtbi.2004.11.038)
84. Salazar JD, Saithong T, Brown PE, Foreman J, Locke JC, Halliday KJ, Carré IA, Rand DA, Millar AJ. 2009 Prediction of photoperiodic regulators from quantitative gene circuit models. *Cell* **139**, 1170–1179. (doi:10.1016/j.cell.2009.11.029)
85. Troein C, Corellou F, Dixon LE, van Ooijen G, O'Neill JS, Bouget FY, Millar AJ. 2011 Multiple light inputs to a simple clock circuit allow complex biological rhythms. *Plant J*. **66**, 375–385. (doi:10.1111/j.1365-313X.2011.04489.x)
86. Song YH, Smith RW, To BJ, Millar AJ, Imaizumi T. 2012 FKF1 conveys timing information for CONSTANS stabilization in photoperiodic flowering. *Science* **336**, 1045–1049. (doi:10.1126/science.1219644)
87. Brancaccio M, Maywood ES, Chesham JE, Loudon AS, Hastings MH. 2013 A Gq-Ca^{2+} axis controls circuit-level encoding of circadian time in the suprachiasmatic nucleus. *Neuron* **78**, 714–728. (doi:10.1016/j.neuron.2013.03.011)
88. Gould PD *et al.* 2013 Network balance via CRY signalling controls the *Arabidopsis* circadian clock over ambient temperatures. *Mol. Syst. Biol*. **9**, 650. (doi:10.1038/msb.2013.7)
89. Dixon LE, Hodge SK, van Ooijen G, Troein C, Akman OE, Millar AJ. 2014 Light and circadian regulation of clock components aids flexible responses to environmental signals. *New Phytol*. **203**, 568–577. (doi:10.1111/nph.12853)
90. Force MM, Robinson NJ. 2014 Encouraging data citation and discovery with the data citation index. *J. Compt-aided Mol. Des*. **28**, 1043–1048. (doi:10.1007/s10822-014-9768-5)
91. International Arabidopsis Informatics Consortium. 2012 Taking the next step: building an *Arabidopsis* information portal. *The Plant Cell* **24**, 2248–2256. (doi:10.1105/tpc.112.100669)
92. PlaSMo 2010 The Plant Systems Modelling portal. See www.plasmo.ed.ac.uk.
93. Akman OE, Watterson S, Parton A, Binns N, Millar AJ, Ghazal P. 2012 Digital clocks: simple Boolean models can quantitatively describe circadian systems. *J. R. Soc. Interface* **9**, 2365–2382. (doi:10.1098/rsif.2012.0080)
94. Aderhold A, Husmeier D, Grzegorczyk M. 2014 Statistical inference of regulatory networks for circadian regulation. *Stat. Appl. Genet. Mol. Biol*. **13**, 227–273. (doi:10.1515/sagmb-2013-0051)
95. Carrera J, Rodrigo G, Jaramillo A, Elena SF. 2009 Reverse-engineering the *Arabidopsis thaliana* transcriptional network under changing environmental conditions. *Genome Biol*. **10**, R96. (doi:10.1186/gb-2009-10-9-r96)
96. Pokhilko A, Ramos JA, Holtan H, Maszle DR, Khanna R, Millar AJ. 2011 Ubiquitin ligase switch in plant photomorphogenesis: a hypothesis. *J. Theor. Biol*. **270**, 31–41. (doi:10.1016/j.jtbi.2010.11.021)
97. Goff SA *et al.* 2011 The iPlant collaborative: cyberinfrastructure for plant biology. *Front. Plant. Sci*. **2**, 34.
98. Knight H, Thomson AJ, McWatters HG. 2008 Sensitive to freezing integrates cellular and environmental inputs to the plant circadian clock. *Plant Physiol*. **148**, 293–303. (doi:10.1104/pp.108.123901)
99. Garwood KL, Taylor CF, Runte KJ, Brass A, Oliver SG, Paton NW. 2004 Pedro: a configurable data entry tool for XML. *Bioinformatics* **20**, 2463–2465. (doi:10.1093/bioinformatics/bth251)
100. Le Novere N *et al.* 2006 BioModels Database: a free, centralized database of curated, published, quantitative kinetic models of biochemical and cellular systems. *Nucleic Acids Res*. **34**, D689–D691. (doi:10.1093/nar/gkj092)

Supporting Information

Contents

Supplementary Methods

Plant materials

The biological materials and allele numbers used in each experiment are shown in Figure 1C.

Growth, harvesting, RNA extraction and analysis

ROBuST dataset (Experiment 1 of Figure 1C)

Seedlings were grown on half-strength Murashige & Skoog media (MS) with 1.2 % agar, without added sucrose. Following 7 days of entrainment under LD cycles of 12h L:12h D at 22°C, seedlings were transferred to 17°C on the same light regime, and on the fifth day at 17°C seedlings were harvested every two hours into 1 ml of RNAlater (Ambion; Austin, Texas, USA). Lighting was 60 µmol/m^2/s white fluorescent light provided in a Binder (Tuttlingen, Germany) temperature-controlled incubator. Biological triplicates were independently sampled. Samples at ZT0 were taken just before lights-on, and samples at ZT12 just after lights-off. All sampling during lights-off was conduction in a temperature-controlled dark room. Total RNA was extracted (GE Healthcare Illustra RNAspin 96 RNA Isolation Kit, Buckinghamshire, UK) according to the manufacturer's instructions. cDNA was synthesized from 1 µg of total RNA (Invitrogen SuperScript VILO cDNA Synthesis kit, Paisley, Scotland) and diluted 1:10 in H_2O. qRT-PCR reactions were carried out and analysed as previously described (1) in technical triplicate. Expression values were normalized to the control transcript ACTIN 7 (ACT7), amplified with primers 5' CAGTGTCTGGATCGGAGGAT 3' and 5' TGAACAATCGATGGACCTGA 3'.

TiMet datasets

a. Plants grown on soil: TiMet rosette and seedling 1 datasets (Experiments 2 and 3 of Figure1C)

Arabidopsis thaliana seeds were sown on wet soil, covered with transparent lids and transferred to growth chambers. Plants were grown in 12 h light / 12 h dark cycles with a light intensity adjusted to 160 µmol $m^{-2}s^{-1}$. Temperature was 20℃ during the light phase and 18℃ during the dark phase. Pots were randomized to decrease positional effect. After a week lids were removed and the excess plants were thinned. After another seven days plants were treated with Nematodes as a biological pest control.

On the 21st day (rosette plants) or 13th day (seedlings) after sowing two biological replicates per time point were harvested and immediately frozen in liquid nitrogen. Each replicate consisted of a pool of 5-7 plants. Sampling was performed with 2h intervals, starting at ZT0, within 5-10 minutes before the given time point. Plant material was ground using a Ball-Mill (Retch, Germany). Around 50 mg of

material from each sample was aliquoted into 2ml microcentrifuge tubes (Eppendorf, Germany). RNA was extracted using the RNeasy Plant Mini Kit (QIAGEN) by following the manufacturer's instructions. Briefly, the RLC buffer (500µL) was added to the frozen plant powder and the mixture was homogenised. RNA standards were added (see below). RNA was eluted from the RNeasy spin column twice, first with 50 µL and then with 30 µL of RNase-free water. The concentration of RNA was determined using the Nano-Drop ND-1000 UV-Vis spectrophotometer (Nano-Drop Technologies).

b. Plants grown in sterile media: TiMet seedling 2 dataset (Experiment 4 of Figure1C)

Surface-sterilized seeds were sown on half-strength Murashige-Skoog media (MS) with 1.2 % agar without addition of sucrose. After 4 days of stratification in the dark at 4℃ plates were transferred to growth chambers and grown for 10 days in 12 light / 12 dark cycles, with light intensity of approx. 100 µmol $m^{-2}s^{-1}$ and temperature of 22℃ during the day and 18℃ during the night. Seedlings were harvested on the 10^{th} day into 2ml Eppendorf tubes and immediately frozen in liquid nitrogen. For each time point, three independent biological replicates were collected; each included 10-20 seedlings. Samples were taken within 10 – 15 min before the given time point. Frozen seedlings were ground using a Ball-Mill (Retch, Germany). RNA was extracted using the RNeasy Plant Mini Kit (QIAGEN) but using half the volume of all buffers. RNA standards were added (see below). In the last step RNA was eluted from the RNeasy spin column once with 20 µL of RNase-free water. The concentration of RNA was determined using the Nano-Drop ND-1000 UV-Vis spectrophotometer (Nano-Drop Technologies).

c. cDNA preparation and analysis

Contaminating DNA was removed from samples using TURBO DNA-free™ kit (Applied Biosystems) by following the manufacturer's instructions. The concentration of RNA was determined using Nano-Drop spectrophotometer. 1µg of DNase treated RNA was used for cDNA synthesis. Reverse transcription used the SuperScript III First-Standard Synthesis System Kit (Invitrogen). Briefly, 1µg of DNase treated RNA was mixed with 2µL of oligo(dT) primers (50µM), 2µL of random hexamers (50ng/µL) and 1µL of dNTP mix (10mM). Mixture of a final volume of 11µL was incubated for 5 min at 65˚C in a Verti 96 Well Thermal Cycler (Applied Biosystems, Deutschland). After cooling down the mixture for 5 min on ice the extension reaction was performed by adding 0.5µL of reverse transcriptase (SuperScript III RT 200 U/µl), 2µL of 10X First strand synthesis buffer, 4µL of $MgCl_2$ (25mM), 2µL of DTT (0.1M) and 0.5µL of RNase OUT (40 U/µL). Incubation for 10 min at 25˚C was followed by 50 min incubation at 50˚C. Next, enzyme was inactivated by heating for 5 min at 85˚C. To digest all RNA that could potentially be left in samples 1 µL RNase H (2 U/µL) was added to the mixture and incubated at 37˚C for 20 min and then for 5 min at 85˚C. Samples were diluted in RNase-free water (dilution 1/5).

The cDNA was used for qRT-PCR reactions to monitor the expression level of 10 core clock genes (*LHY, CCA1, TOC1, PRR9, PRR7, PRR5, GI, ELF3, ELF4* and *LUX*). To control the quality of performed reactions, four pairs of primers encoding housekeeping genes (*ACT2 155, ACT2 633, GAPDH 3', GAPDH 5'*) were included to the measurements. Primer sequences are listed in Supplementary Table 2. To allow absolute quantification, 8 pairs of primers from the ArrayControl *RNA Spikes* (Applied Biosystems) were included (see below). The 22 pairs of primers were dispensed (200nM of each primer) into 384-well plates for using PerkinElmer Evolution P3 Precision Pipetting Platform (PerkinElmer Life Science, Rodgau-Jügesheim, Germany). PCR mix was prepared by adding 0.5µL of cDNA and 2.5µL of Power SYBR Green PCR Master Mix (Applied Biosystems, Deutschland) to already prepared primers. The qRT-PCR reactions were carried out following the recommended thermal profile: 2 min at 50˚C, 10 min at 95˚C, followed by 40 cycles of 95˚C for 15 s and 60 ˚C for 1 min, in an ABI PRISM 7900 HT sequence detection system (Applied Biosystems Deutschland, Darmstadt, Germany). The specificity of the amplifications was tested by heating from 60˚C to 95˚C with a speed of 1.9 ˚C min^{-1}, resulting in melting curves. Data analysis was performed using SDS 2.4 software (Applied Biosystems Deutschland). Data were normalised on the basis of results obtained from measurements of standard material that was included in all performed experiments. The standard samples were collected from *Arabidopsis thaliana* plants, ecotype Col-0, grown on soil in a glasshouse.

d. Data calibration to absolute values

The transcript data are expressed in RNA copy number per cell. This absolute quantification of the transcripts level was achieved using artificial poly(A)$^+$ RNAs (ArrayControl *RNA Spikes* - Applied Biosystems) as internal standards. Eight different artificial mRNA spikes with known concentration (Supplementary Table 1) were mixed and the same amount of the spikes mix was added to all tested samples at the first step of the RNA extraction procedure (after adding the RLC buffer to the frozen plant material, see above). The efficiency and the C_t values of all 8 spikes were used to generate a standard curve for each sample. Each measured data point was plotted against the standard curve to calculate the concentration of mRNA in units of copy number per gram fresh weight (copy number / g FW). The procedure is very similar to our earlier report (2), which also addressed the accuracy of the measurements. Our results are in line with their conclusion that, for a single timepoint with achievable replication, "Precise quantification of changes of [less than] two-fold is difficult using qRT–PCR.". Adjacent timepoints and successive daily cycles in circadian data provide greater support than the single-timepoint assays in (2). Rigorous assessment of the uncertainties will require more sophisticated statistical models, as the system's behaviour is not independent at successive, 2-h timepoints.

To determine the cell number per g FW, the genome copy number per gFW was quantified. For this purpose artificial DNA spikes were added to the extract during DNA extraction (at the beginning of the protocol). Next, PCR reactions with primers for genes that are known to have only a single copy

per genome (e.g. mitochondrial 26S ribosomal RNA protein, NADH dehydrogenase subunit 9, NAD(P)H dehydrogenase subunit H protein) were performed. The ploidy level of the samples was estimated using flow cytometry. Finally, the genome copy number per g FW was divided by the ploidy level. The resulting number (25.000.000 copy number/g FW) was used to express metabolite and transcript data.

McWatters dataset (Experiment 5 of Figure 1C)

Seedlings were grown on sterile media containing 3% sucrose. Entire seedlings including roots were harvested every 3h. RNA was extracted, amplified and analysed, all using methods previously described (3).

Edwards dataset (Experiment 6 of Figure 1C)

Seedlings were grown on sterile media containing 3% sucrose. Entire seedlings including roots were harvested every 2h. RNA was extracted and analysed as described (4).

Southern dataset (Experiment 7 of Figure 1C)

Seedlings were grown on sterile media containing 3% sucrose, harvested every 3h with additional sampling times around light-dark transitions; RNA was extracted, amplified and analysed, as described (5).

Evaluation of datasets

The larger data sets reported here were acquired using automated, quantitative RT-PCR platforms that were established as shared facilities for research centres in Golm and Edinburgh. The experiments remained laborious and costly, despite the automation and reduced reagent costs from small assay volumes; further miniaturisation of these assays shows promise for future studies (as in 6). Large-scale data cannot usually be acquired with the same uniformity as small-scale datasets. Replacing individual measurements with supplementary experiments to improve technical quality is infeasible, because the broad scope of genotypes, conditions and timepoints in the original studies makes such experiments expensive relative to the small number of improved data points, and introduces a further source of variation. Thus we note technical variation in order to inform subsequent analysis, reinforcing the point that only a small proportion of the data were affected. RNAs with low amplitude regulation (*TOC1, ELF3*) or low expression levels (*PRR9*) are most obviously affected. Automated liquid handling avoided the sample-to-sample variation of manual pipetting in the earlier, Southern data (Supplementary Figure 5E, 5F) but risked introducing larger-scale effects. Three issues affected multiple samples. One timepoint (ZT24) in the ROBuST data was discarded for several genotypes due

to a harvesting error; ZT24 data are expected to be very similar to ZT0 but the tissue is one day older. Some technical replicates in ROBuST were discarded and repeated wholesale when a trend was discovered across multiple samples, due to a progressive liquid handling error in the robot used in PCR setup. The first Col-0 samples in the TiMet rosette dataset showed high biological variability due to harvesting or calibration, so the entire first 24h of the timeseries were replaced by a supplementary experiment (shown as experiment 2B in Figure 1C).

No molecular phenotype was detected when the *toc1* mutant was tested under red light in the Southern data set (data not shown). The strong *toc1-2* mis-sense allele that was used in this study causes a splicing defect (7). The expected change in the size of the *TOC1* transcript was detected using the method described (7) on our RNA samples, confirming their genotype (8). *toc1-2* seedlings do show hypocotyl elongation defects when grown under red light on media without exogenous sucrose (9), so the absence of molecular phenotype is possibly due to 3% sucrose in our media. The *toc1-9* and *toc1-100* alleles tested under white light in the ROBuST and TiMet data sets gave the expected molecular phenotypes.

We found no consistent effect on the RNA profiles from normalisation to endogenous control RNAs. TiMet rosette data were normalised to absolute, external standards (Figure 1) or to internal controls (Figure 3), for comparison to the profiles from other data sets. The profiles were very similar in both analyses, even for features that varied across experiments. In the GI profile, for example, the minor peak at ZT2 was 20% of the major peak at ZT8 in Figure 1 in Col in Figure 1 (18% in Figure 3), or 11% (10%) in Ws. The 1-2% differences were much less than the biological variation (see Figure 1).

Supplementary Analysis

Interpretation of Phase-Plane Diagrams

Phase plane diagrams plot the levels of two components against each other (Figure 7), exactly as in a scatter plot used to test for correlation. The data in scatter plots do not usually have a meaningful sequence. Timeseries do, so the data points in a phase plane diagram are connected by a line that represents their time sequence. Data symbols for ZT0 and ZT12 are enlarged to provide time references, because sample times are not directly plotted. Rhythmic profiles in phase lead to a diagonal plot with a positive gradient, for example for *GI* and *TOC1* expression (Figure 7A), whereas rhythms 90 or 270 degrees out of phase produce a circular plot. *GI* and *TOC1* expression reached peak and trough levels at overlapping timepoints, elongating the plot along the positive diagonal. The plots form an open shape rather than a line, because *GI* rose without (before) *TOC1*, especially in Col plants of the TiMet and ROBuST data sets, without exogenous sucrose. High *TOC1* occurred after

high *GI*, particularly in Ws plants of the TiMet data sets. This relative timing is of course easy to see in conventional timeseries plots, and has been noted in many past studies.

Rhythms 180 degrees out of phase yield a right-angled plot on a linear scale, or a diagonal of gradient -1 on a logarithmic scale, illustrated in the plots of *CCA1* and *TOC1* RNA (Figures 7B, 7C) The logarithmic scale shows that *CCA1* expression rises over 100-fold along roughly horizontal lines, indicating little effect on *TOC1*. In contrast, the rise in *TOC1* expression directly correlates with falling *CCA1,* resulting in diagonals with negative gradients (Figure 7C). Linear scale plots might best represent potential protein synthesis, which is usually assumed to increase linearly with mRNA level; hence linear plots suggest likely effects on downstream targets. On the other hand, logarithmic scale plots reveal the effects of upstream regulators, even at low RNA levels that are indistinguishable on a linear scale.

The dependence of an interaction of two genes upon a third regulator was strikingly illustrated by plotting the profiles of *PRR9* and *ELF4*, which peak far out of phase in the wild type (Figure 7D). Starting from ZT0, acute light activation of *PRR9* drives peak expression at ZT2-6 while *ELF4* expression is minimal. *ELF4* expression rises to peak at ZT10 as *PRR9* falls, consistent with some contribution to repressing *PRR9*. *ELF4* expression falls at night (red dashed line) while *PRR9* expression is minimal. Data from LL (filled symbols) suggest a negative correlation in the subjective night, when *ELF4* falls as *PRR9* rises. In the *lhy cca1* double mutant under LD cycles (Figure 7E, open symbols), *PRR9* is partially de-repressed at ZT0, but remains out of phase with *ELF4.* However, the two genes are co-regulated for part of the cycle under LL, creating a diagonal with a positive gradient (red dashed line, Figure 6F).

Phase plane diagrams for the *prr7 prr9* double mutant (Figure S6) showed that *ELF4* expression rose while *CCA1* (and *LHY*, not shown) were still significantly expressed at the end of the day, suggesting that not only CCA1 and LHY but also the PRRs repress *ELF4* in the wild type. Removing *PRR9* and *PRR7* also revealed simpler correlations of *PRR5* expression with *CCA1* and *ELF4* (Figures S6E, S6H).

Model versioning and optimisation

We have adapted the Community Earth System Model version-naming convention (10) (www2.cesm.ucar.edu/models) to describe version of our clock models. Models are named as Axxxx.Y.Z., where A is a letter of the model author's surname, xxxx is the year of submission, Y is a version number marking a significant change in the model that alters its dynamics such as a new

parameter set, Z is a minor change that does not alter the model's dynamics such as the refactoring of the light input function. The version identifier should link to a unique identifier in at least one model repository.

Model optimisation used SBSIvisual version 1.4.5 (11) and SBSInumerics version 1.2, which are both available from Sourceforge. Model P2011.1.2 (PLM_64, version 4) was optimised using SBSI's Parallel Genetic Algorithm, with a range of parameter constraints (Table 2). Starting parameter sets were chosen as normal (P2011.2.1) or logarithmic values (P2011.3-P2011.6) within the stated ranges, either randomly (P2011.3-P2011.6) or from a quasi-random Sobol series (P2011.2.1). The departure of each model's simulations of wild-type and mutants from the normalised TiMet rosette data was evaluated using SBSI's chi-square cost function, and their departure from measured period values under constant light was evaluated using SBSI's FFT cost function. SBSInumerics v1.2 estimates the period of simulated timeseries with greater precision than v1.1. SBSInumerics does not specifically cost the amplitude of the simulated timeseries, which are constrained only by the match to the RNA data. The results (Figure 9) suggest that small discrepancies in simulated amplitude are better tolerated in the costing than discrepancies in timing, matching our priorities. Moreover, our choice of Hill coefficients is very conservative (all set at 2), restricting the nonlinearity of simulated gene regulation and tending to reduce the amplitudes of the simulated RNA profiles. The >100-fold relative amplitudes observed for some clock RNAs suggest much greater non-linearity of regulation in vivo.

Optimisation job .599 tested 5000 randomly-generated parameter sets and optimised the best solutions in a population of 200 models over 599 generations; computation time was 6 hours on a server with eight Intel Xeon processing cores. Job t40 tested randomly-generated parameter sets before optimising the best solutions as above; computation time was 8.5 hours using 4096 processing cores on the UK national supercomputing resource HECToR. The parameter constraints and optimised parameter values are listed in the SBML files (see Data, model and code accessibility).

Supplementary Figure Legends

Supplementary Figure 1. Overview of the clock gene circuit

The clock gene circuit summarised in the Activity-Flow language of SBGN v1.0 (12), with the principal light inputs and regulatory interactions in the P2012 model (13). The repressilator is denoted by green lines; morning loop components are filled yellow; evening loop components are filled blue.

Supplementary Figure 2. Detailed schema of the P2011 model

The clock gene network in the P2011 model (14), represented in the SBGN Process Description language. All connections in the model are depicted, along with the logic inherent in the form of the equations. Coloured edges correspond to different parts of the model: Yellow edges - Light inputs. Green edges - Morning loop. Blue edges - Evening loop. Purple edges – connections among loops.

Supplementary Figure 3. Logarithmic plots of clock gene expression in wild-type plants under LD cycles

Transcript levels in Col-0 and Ws-2 wild types under LD 12:12 were measured by qRT-PCR, in experiment 2 (TiMet ros) including eight external RNA standards to allow absolute quantification in Col-0 and Ws-2 (A, C, E) and in experiment 1 (ROBuST) normalised to the *ACTIN7* control in Col-4 and Ws-2 (B, D, F). Data represent transcripts of (A, B) *LHY* and *CCA1*, (C, D) *PRR9*, (E, F) *TOC1* and *GI*. Error bars show SD, for 2-3 biological replicates. Figure 2 shows the same data on a linear scale.

Supplementary Figure 4. RNA profiles under DD

RNA profiles of (A) *CCA1* and (B) *GI* expression from the Edwards dataset for seedlings on sucrose (4), under LD cycles of 6, 12 or 18h photoperiod followed by DD (legend, panel B). RNA profiles from the TiMet rosette dataset for plants in 12h photoperiod, transferred to DD, for (C) *PRR7,* (D) *PRR9* expression. Higher trough levels are observed in DD than under LD, often more than ten-fold higher. (A), (B) Data shown are relative to the *ACTIN2* control; (C)-(D) data are calibrated to RNA copy number per cell. Means of two biological replicates per timepoint are shown, error bar is SD. Open box, light interval; filled box, dark interval, A and B, coloured as for legend.

Supplementary Figure 5. Mutant effects are consistent among data sets.

RNA profiles from the ROBuST dataset for seedlings under LD cycles show (A) the slower fall of *PRR5* expression in the *gi-11* mutant compared to wild type, persisting from ZT10-16h (logarithmic scale, B); (C) earlier and lower peak expression of *TOC1* in the *lhy cca1* double mutant; (D) lower expression of *ELF3* in the *gi* mutant, especially at ZT8-10h; (E) persistent expression of *CCA1* in the prr7 prr9 double mutant, with an early rise in *prr7* and delayed fall in *prr9*. RNA profiles from the Southern data for *elf3* and *elf4* mutant seedlings under red light-dark cycles show (F) persistently high and noisy expression of *GI*; (G) expression of *CCA1* that falls from the level in Ws

to *elf4*, which remains rhythmic in constant conditions, and falls further to *elf3*, which is arrhythmic. A-D show means of three biological replicates per timepoint, error bars are SEM. E, F show one of two replicate experiments with similar results. Plots in panels C and D are from BioDare.

Supplementary Figure 6. Phase plane diagrams reveal altered regulation in *prr7 prr9* mutants.

RNA profiles of Figure 5 are represented as phase plane diagrams on logarithmic scales, plotting data for *ELF4* and *CCA1* (A) in wild-type Col plants under LD and LL and (B) in Col plants under LD and *prr7 prr9* double mutants under LD and LL, with (C) the LD data for both genotypes on linear scales.

(D)-(E) show data for *PRR5* and *CCA1* (D) in wild-type Col plants under LD and LL and (E) in Col plants under LD and *prr7 prr9* double mutants under LD and LL. (E) Red dashed line marks anti-correlated levels during the subjective night in the double mutant in LL.

(F)-(H) show data for *ELF4* and *PRR5* (F) in wild-type Col plants under LD and LL, (G) in Col plants under LD and *prr7 prr9* double mutants under LD and (H) for *prr7 prr9* double mutants under LD and LL. (H) Red dashed lines mark highly correlated rise and fall of *PRR5* and *ELF4* levels in the double mutant under LL, whereas the relationship was more complex in the wild type. Larger markers indicate ZT0(24) and ZT12(36) datapoints in LD (LL), arrows indicate the direction of time.

Supplementary Figure 7. Regulation of clock-related genes in low-sugar conditions.

RNA microarray data (15, 16) displayed by the online tool (http://mapman.mpimp-golm.mpg.de/supplement/xn/) from treatments with light, CO_2-free air (ΔCO_2), DD (eXtended Night), or the starchless *pgm* mutant, for (A) *LHY*, *PRR7* (green), *PRR5* and *TOC1*; (B) *ZTL, FKF1* and *LKP2*. (A) Arrows mark higher *PRR7* levels in sugar-limiting DD and *pgm* relative to control in LD cycle, repression by re-supply of high exogenous sugar (3 Suc) but less effect from resupply of normal air (350ppm CO_2). (B) Arrows mark higher levels of *ZTL, FKF1* and *LKP2* RNA in DD and *pgm.*

Supplementary Table Legends

Supplementary Table 1. mRNA calibration standards.

Concentration of artificial mRNA spikes (number of copies per extract) added to each sample as an internal standard to allow the quantification of RNA copy number.

Supplementary Table 2. qRT-PCR primer sequences.

The PCR primer sequences used in the TiMet studies are listed below. The PCR primer sequences used in the ROBuST data set are listed in the public record for each transcript on BioDare (please see Data Accessibility), and the primer sequences for other studies are listed in their original publications and in the BioDare records (please see Data Accessibility).

Supplementary References

1. Dixon LE, Knox K, Kozma-Bognar L, Southern MM, Pokhilko A, Millar AJ. Temporal repression of core circadian genes is mediated through EARLY FLOWERING 3 in Arabidopsis. Curr Biol. 2011;21(2):120-5.
2. Piques M, Schulze WX, Hohne M, Usadel B, Gibon Y, Rohwer J, et al. Ribosome and transcript copy numbers, polysome occupancy and enzyme dynamics in Arabidopsis. Mol Syst Biol. 2009;5:314.
3. Knight H, Thomson AJ, McWatters HG. Sensitive to freezing6 integrates cellular and environmental inputs to the plant circadian clock. Plant Physiol. 2008;148(1):293-303.
4. Edwards KD, Akman OE, Knox K, Lumsden PJ, Thomson AW, Brown PE, et al. Quantitative analysis of regulatory flexibility under changing environmental conditions. Mol Syst Biol. 2010;6:424.
5. Locke JC, Southern MM, Kozma-Bognar L, Hibberd V, Brown PE, Turner MS, et al. Extension of a genetic network model by iterative experimentation and mathematical analysis. Mol Syst Biol. 2005;1:2005 0013.
6. Huang W, Perez-Garcia P, Pokhilko A, Millar AJ, Antoshechkin I, Riechmann JL, et al. Mapping the core of the Arabidopsis circadian clock defines the network structure of the oscillator. Science. 2012;336(6077):75-9.
7. Strayer C, Oyama T, Schultz TF, Raman R, Somers DE, Mas P, et al. Cloning of the *Arabidopsis* clock gene *TOC1*, an autoregulatory response regulator homolog. Science. 2000;289(5480):768-71.
8. Southern MM. Mutants in the Arabidopsis Circadian Clock: Genetic Approaches to Explore Circadian Mechanisms in the Model Higher Plant: University of Warwick; 2005; Ph.D. thesis.
9. Ito S, Nakamichi N, Nakamura Y, Niwa Y, Kato T, Murakami M, et al. Genetic linkages between circadian clock-associated components and phytochrome-dependent red light signal transduction in Arabidopsis thaliana. Plant Cell Physiol. 2007;48(7):971-83.
10. Levis S, Bonan GB, Kluzek E, Thornton PE, Jones A, Sacks WJ, et al. Interactive Crop Management in the Community Earth System Model (CESM1): Seasonal Influences on Land-Atmosphere Fluxes. J Climate. 2012;25(14):4839-59.
11. Adams R, Clark A, Yamaguchi A, Hanlon N, Tsorman N, Ali S, et al. SBSI: an extensible distributed software infrastructure for parameter estimation in systems biology. Bioinformatics. 2013;29(5):664-5.
12. Le Novere N, Hucka M, Mi H, Moodie S, Schreiber F, Sorokin A, et al. The Systems Biology Graphical Notation. Nat Biotechnol. 2009;27(8):735-41.
13. Pokhilko A, Mas P, Millar AJ. Modelling the widespread effects of TOC1 signalling on the plant circadian clock and its outputs. BMC Syst Biol. 2013;7:23.
14. Pokhilko A, Fernandez AP, Edwards KD, Southern MM, Halliday KJ, Millar AJ. The clock gene circuit in Arabidopsis includes a repressilator with additional feedback loops. Mol Syst Biol. 2012;8:574.
15. Blasing OE, Gibon Y, Gunther M, Hohne M, Morcuende R, Osuna D, et al. Sugars and circadian regulation make major contributions to the global regulation of diurnal gene expression in Arabidopsis. Plant Cell. 2005;17(12):3257-81.
16. Usadel B, Blasing OE, Gibon Y, Retzlaff K, Hohne M, Gunther M, et al. Global Transcript Levels Respond to Small Changes of the Carbon Status during Progressive Exhaustion of Carbohydrates in Arabidopsis Rosettes. Plant Physiol. 2008;146(4):1834-61.

Supplementary Tables

Supplementary Table 1

Concentration of artificial mRNA spikes (number of copies per extract) added to each sample as an internal standard to allow the quantification of RNA copy number.

	Spike1	**Spike 2**	**Spike 3**	**Spike 4**	**Spike 5**	**Spike 6**	**Spike 7**	**Spike 8**
Copies per extract	6.08 E+09	1.52 E+09	4.56 E+08	1.14 E+08	2.94 E+07	3.04 E+05	2.58 E+06	7.60 E+05

Supplementary Table 2. qRT-PCR primer sequences.

The PCR primer sequences used in the TiMet studies are listed below, followed by the PCR primers for the Southern dataset. The PCR primer sequences used in the ROBuST data set are listed in the public record for each transcript on BioDare (please see Data Accessibility), and the primer sequences for other studies are listed in their original publications and/or in the BioDare records.

Primers for the TiMet datasets.

Product	CODE	SEQUENCE	Comments
Spike 1	H251-A1780s1-f1	GATGCCCGACCATCATTTAG	
	H252-A1780s1-r1	GTGAGGGTAATGTCGCGTTC	
Spike 2	H253-A1780s2-f1	ATTGCGCTCGCCATATACAC	
	H254-A1780s2-r1	GCTGGGATCAGGAGGAGAAG	
Spike 3	H255-A1780s3-f1	GATCGTTTGCCTGCATTACC	
	H256-A1780s3-r1	GAGAGCGTCAGCCATACCAC	
Spike 4	H257-A1780s4-f1	TACGTCGCACAACCACAATC	
	H258-A1780s4-r1	CAGCGCCACTAACCCACTAC	
Spike 5	H302-S5f-2	ACAAAGGCAGCGTTGAAAAC	
	H301-S5r-1	TAGTGTCTGCACGCCATACC	
Spike 6	Spike-6f-2	CGCAAAGTCTCTCCTCTTGG	
	Spike-6r-2	CAGTAGCCATTGCGGAAGAT	
Spike 7	H313-S7f-3	CTGAACCAGACTGCACATGG	
	H314-S7r-3	ACGCTCATGGGCTTGTTTAT	
Spike 8	H315-S8f-3	TCATTAAAGCGGAAGGCAAT	
	H316-S8r-3	AAATCTTCCAGCACCGTCAG	
GAPDH 3'	H278-GAPDH3	TTGGTGACAACAGGTCAAGCA	
	H279-GAPDH3	AAACTTGTCGCTCAATGCAATC	
GAPDH 5'	H280-GAPDH5	TCTCGATCTCAATTTCGCAAAA	
	H281-GAPDH5	CGAAACCGTTGATTCCGATTC	
ACT2 155	H282-155-ACT2	AACTCTCCCGCTATGTATGTCGC	
	H283-155-ACT2	CAATACCGGTTGTACGACCACTG	
ACT2 633	H284-633-ACT2	ACTTTCATCAGCCGTTTTGA	

	H285-633-ACT2	ACGATTGGTTGAATATCATCAG	
LHY	F019-LHY-f	TGCCTCAAAGCTTTTCGCCTCCT	
	F020-LHY-r	GTCTGCAGCACAAGAATCCTGGCT	
CCA1	F027-CCA1-f	TCCAATGCACGCCGCAGTAGAA	
	F028-CCA1-r	AGGCAATTCGACCCTCGTCAGACA	
PRR9	F037-PRR9-f	AGCTAGCAGAACAACGTCCTCGAGT	
	F038-PRR9-r	CGTCTGAATTCACGGTTCGCACGA	
PRR9	JF309-PRR9-F	GATTGGTGGAATTGACAAGC	primers from A. Millar
	JF310-PRR9-R	TCCTCAAATCTTGAGAAGGC	
PRR7	F045-PRR7-f	AGAGGTGCTTCCGAAAGAAGGTACGA	
	F046 - PRR7-r	ACGCACAAATTGGCCTCGCACT	
PRR5	F051-PRR5-f	TGCAATGGCTCCTGCTTCACTCTC	
	F052-PRR5-r	ACTGTACTCATGCGGGCTAACGGA	
TOC1	F073-TOC1-f	TGATGGATCGGGTTTCTCTGCACCA	
	F074-TOC1-r	TGAGGCATCATGGCTGCTGATTGC	
LUX	F077-LUX-f	CAGCGGTAATGTTGGAGTGCCGAT	
	F078-LUX-r	TGGCATCTGCATCATCTGTTGCGT	
GI	F083-GI-f	TGCGGGCAACTGATGGAATGCT	
	F084-GI-r	TGCTCTTGCCGTGGCTTCAAGT	
ELF4	F091-ELF4-f	AGTTTCTCGTCGGGCTTTCACGGT	
	F092-ELF4-r	TAAGCTCTAGTTCCGGCAGCACCA	
ELF3	F099-ELF3-f	ACAACAAGAGATGGGGGAGGAGTGAC	
	F100-ELF3-r	ACTCGCGAGCTTTGCGTTGTGA	
ELF3	JF576-ELF3-F	CATTCGCAGCCGTTGATGAGG	from Coluccio et al. J. Exp.Bot, 2011
	JF577-ELF3-R	TGTTCTTGTCGTCGTTGTGGTTG	

Primers for the Southern dataset (8).

Product	Forward primer	Reverse primer
ACT2	CAGTGTCTGGATCGGAGGAT	TGAACAATCGATGGACCTGA
LHY	CAACAGCAACAACAATGCAACTAC	AGAGAGCCTGAAACGCTATACGA
CCA1	CTGTGTCTGACGAGGGTCGAA	ATATGTAAAACTTTGCGGCAATACCT
GI	AATTCAGCACGCGCCTATTG	GTTGCTTCTGCTGCAGGAACTT
TOC1	ATCTTCGCAGAATCCCTGTGATA	GCACCTAGCTTCAAGCACTTTACA
ELF3	GGAAAGCCATTGCCAATCAA	ATCCGGTGATGCAGCAATAAGT
ELF4	CGACAATCACCAATCGAGAATG	AATGTTTCCGTTGAGTTCTTGAATC

Supplementary Figure 1

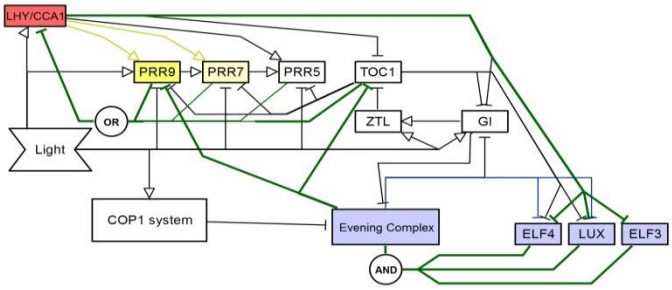

Supplementary Figure 1. Overview of the clock gene circuit

The clock gene circuit summarised in the Activity-Flow language of SBGN v1.0 (Le Novere *et al.*, 2009), with the principal light inputs and regulatory interactions in the P2012 model (Pokhilko *et al.*, 2013). The repressilator is denoted by green lines; morning loop components are filled yellow; evening loop components are filled blue.

Supplementary Figure 2

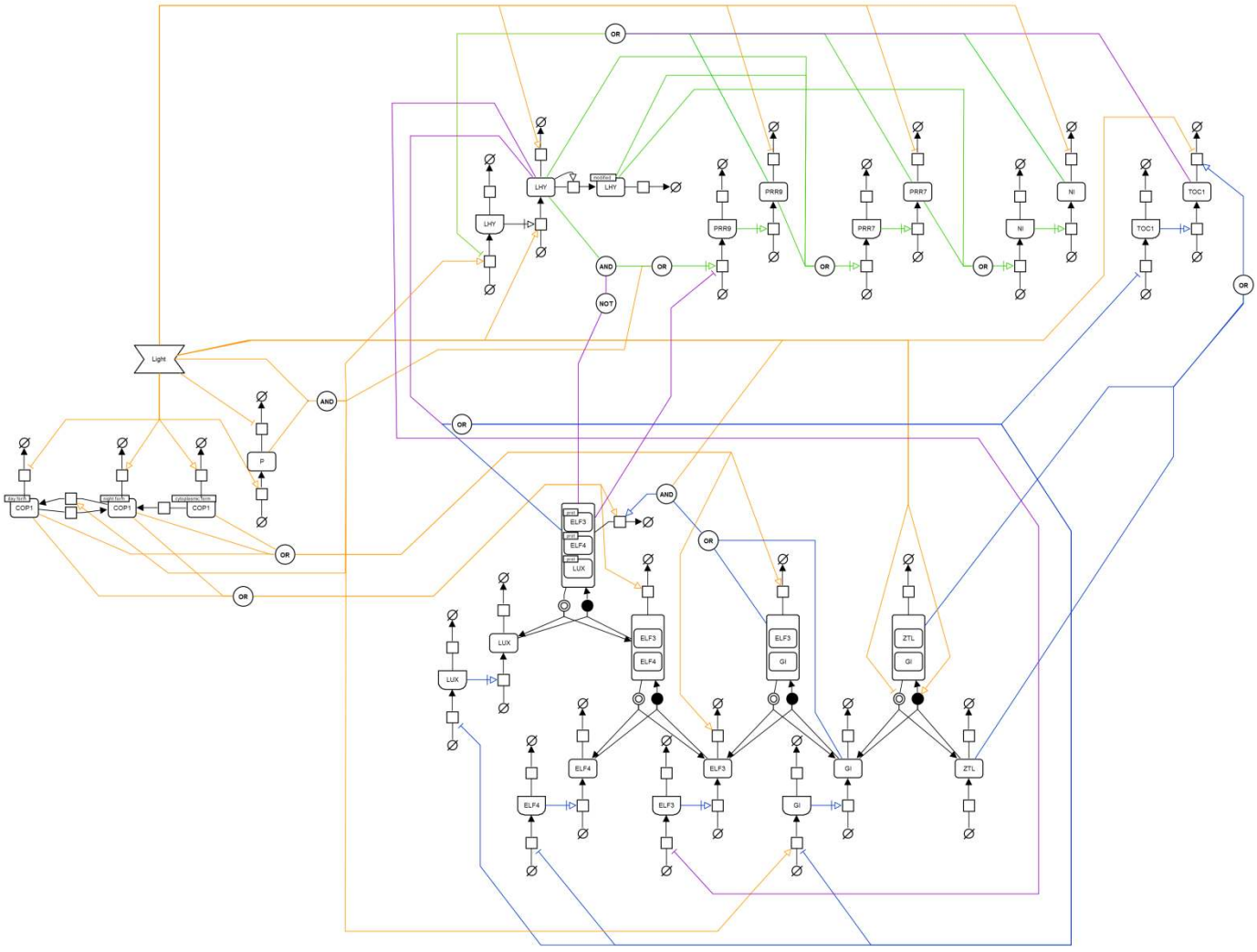

Supplementary Figure 2. Detailed schema of the P2011 model

The clock gene network in the P2011 model (Pokhilko *et al.*, 2012), represented in the SBGN Process Description language. All connections in the model are depicted, along with the logic inherent in the form of the equations. Coloured edges correspond to different parts of the model: Yellow edges - Light inputs. Green edges - Morning loop. Blue edges - Evening loop. Purple edges – connections among loops.

Supplementary Figure 3

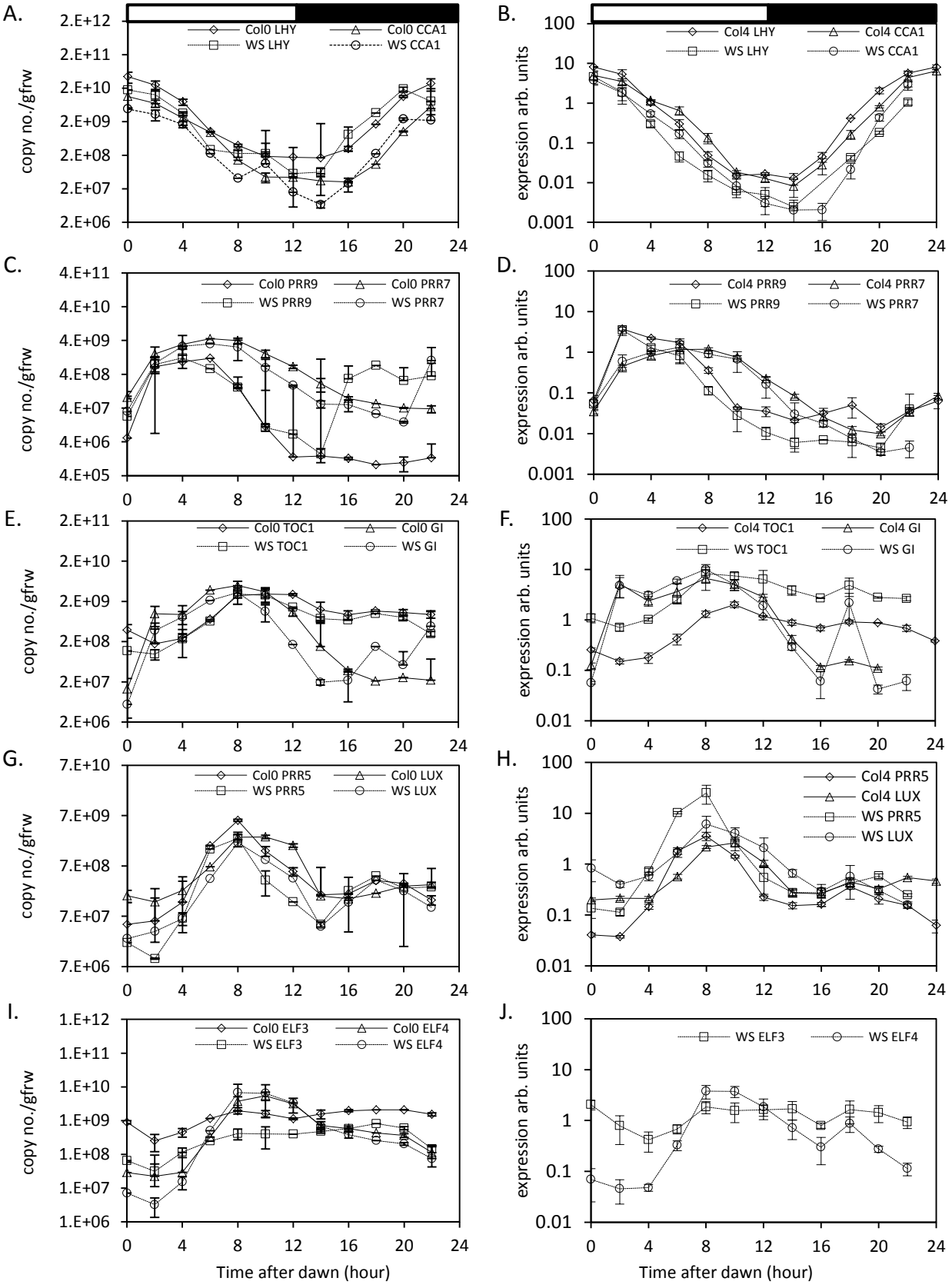

Supplementary Figure 3. Logarithmic plots of clock gene expression in wild-type plants under LD cycles
Transcript levels in Col-0 and Ws-2 wild types under LD 12:12 were measured by qRT-PCR, in experiment 2 (TiMet ros) including eight external RNA standards to allow absolute quantification in Col-0 and Ws-2 (A, C, E) and in experiment 1 (ROBuST) normalised to the *ACTIN7* control in Col-4 and Ws-2 (B, D, F). Data represent transcripts of (A, B) *LHY* and *CCA1*, (C, D) *PRR9*, (E, F) *TOC1* and *GI*. Error bars show SD, for 2-3 biological replicates. Figure 2 shows the same data on a linear scale.

Supplemental Figure 4

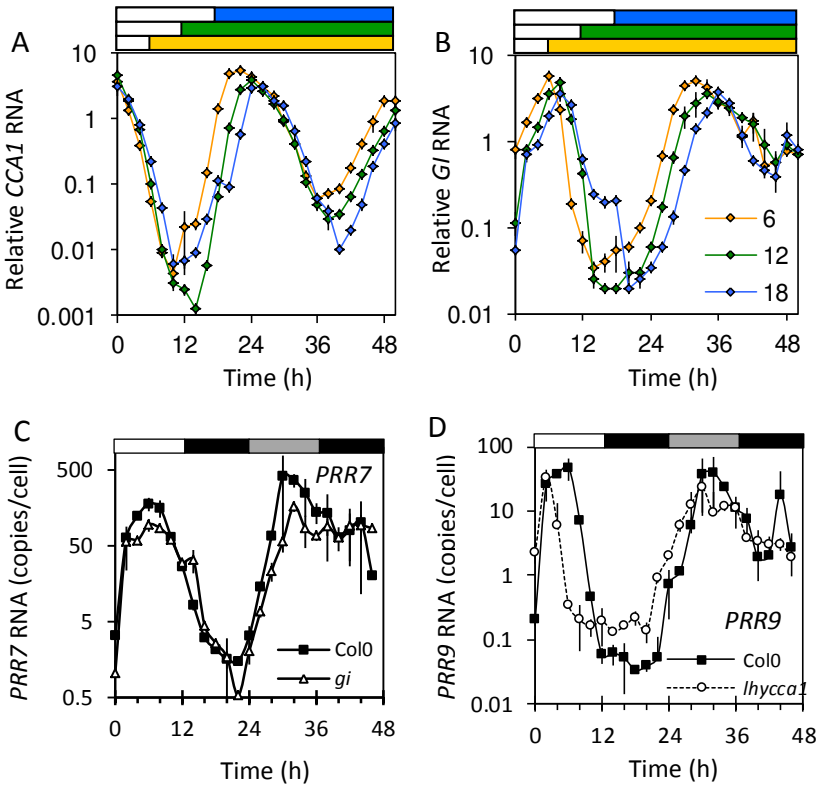

Supplementary Figure 4. RNA profiles under DD

RNA profiles of (A) *CCA1* and (B) *GI* expression from the Edwards dataset for seedlings on sucrose (Edwards *et al.*, 2010) under LD cycles of 6, 12 or 18h photoperiod followed by DD (legend, panel B). RNA profiles from the TiMet rosette dataset for plants in 12h photoperiod, transferred to DD, for (C) *PRR7,* (D) *PRR9* expression. Higher trough levels are observed in DD than under LD, often more than ten-fold higher. (A), (B) Data shown are relative to the *ACTIN2* control; (C)-(D) data are calibrated to RNA copy number per cell. Means of two biological replicates per timepoint are shown, error bar is range. Open box, light interval; filled box, dark interval, A and B, coloured as for legend.

Supplementary Figure 5

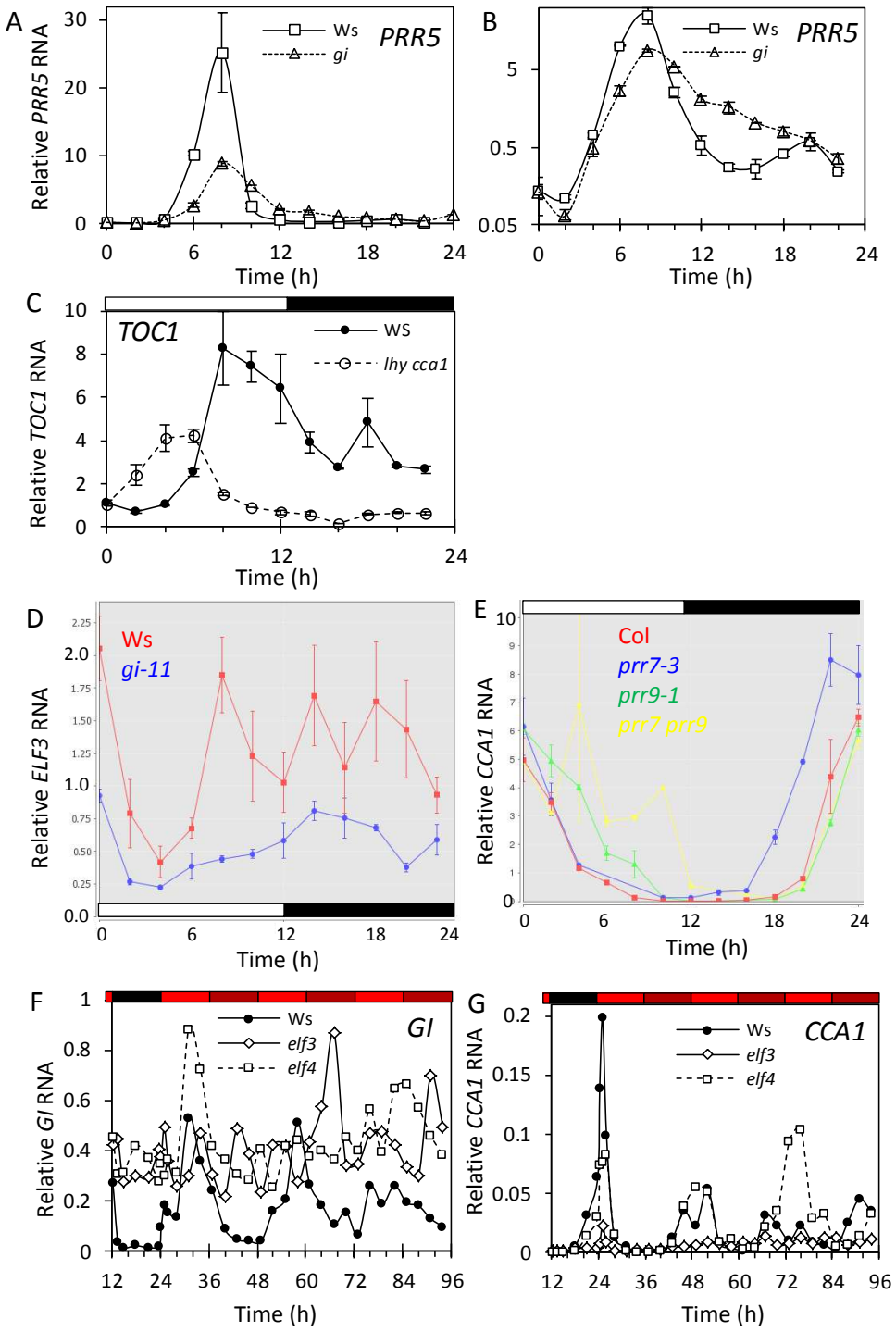

Supplementary Figure 5. Mutant effects are consistent among data sets.
RNA profiles from the ROBuST dataset for seedlings under LD cycles show (A) the slower fall of *PRR5* expression in the *gi-11* mutant compared to wild type, persisting from ZT10-16h (logarithmic scale, B); (C) earlier and lower peak expression of *TOC1* in the *lhy cca1* double mutant; (D) lower expression of *ELF3* in the *gi* mutant, especially at ZT8-10h; (E) persistent expression of *CCA1* in the prr7 prr9 double mutant, with an early rise in *prr7* and delayed fall in *prr9*. RNA profiles from the Southern data for *elf3* and *elf4* mutant seedlings under red light-dark cycles show (F) persistently high and noisy expression of *GI*; (G) expression of *CCA1* that falls from the level in Ws to *elf4*, which remains rhythmic in constant conditions, and falls further to *elf3*, which is arrhythmic. A-D show means of three biological replicates per timepoint, error bars are SEM. E, F show one of two replicate experiments with similar results. Plots in panels C and D are from BioDare.

Supplementary Figure 6

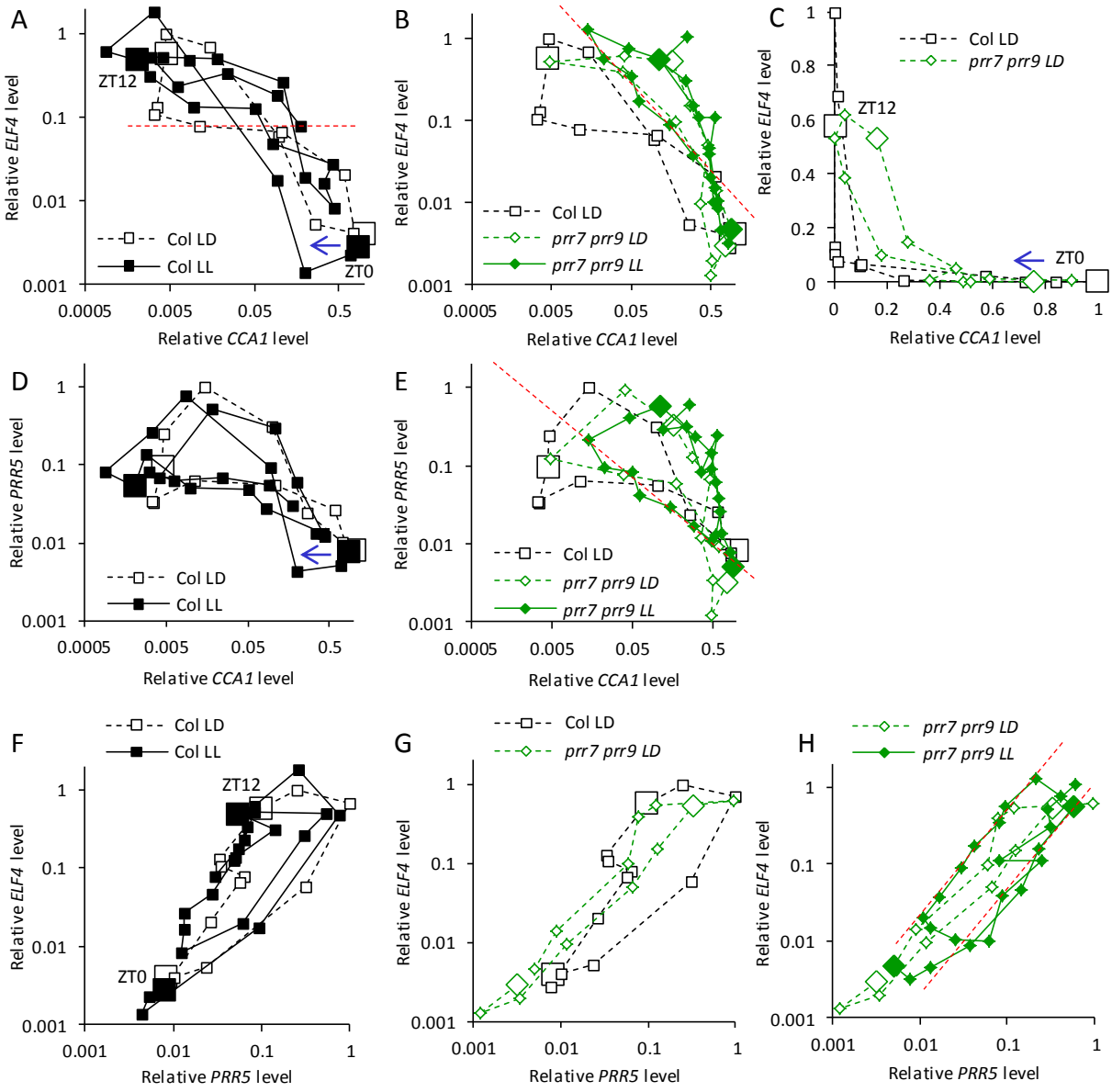

Supplementary Figure 6. Phase plane diagrams reveal altered regulation in *prr7 prr9* mutants.
RNA profiles of Figure 5 are represented as phase plane diagrams on logarithmic scales, plotting data for *ELF4* and *CCA1* (A) in wild-type Col plants under LD and LL and (B) in Col plants under LD and *prr7 prr9* double mutants under LD and LL, with (C) the LD data for both genotypes on linear scales.
(D)-(E) show data for *PRR5* and *CCA1* (D) in wild-type Col plants under LD and LL and (E) in Col plants under LD and *prr7 prr9* double mutants under LD and LL. (E) Red dashed line marks anti-correlated levels during the subjective night in the double mutant in LL.
(F)-(H) show data for *ELF4* and *PRR5* (F) in wild-type Col plants under LD and LL, (G) in Col plants under LD and *prr7 prr9* double mutants under LD and (H) for *prr7 prr9* double mutants under LD and LL. (H) Red dashed lines mark highly correlated rise and fall of *PRR5* and *ELF4* levels in the double mutant under LL, whereas the relationship was more complex in the wild type. Larger markers indicate ZT0(24) and ZT12(36) datapoints in LD (LL), arrows indicate the direction of time.

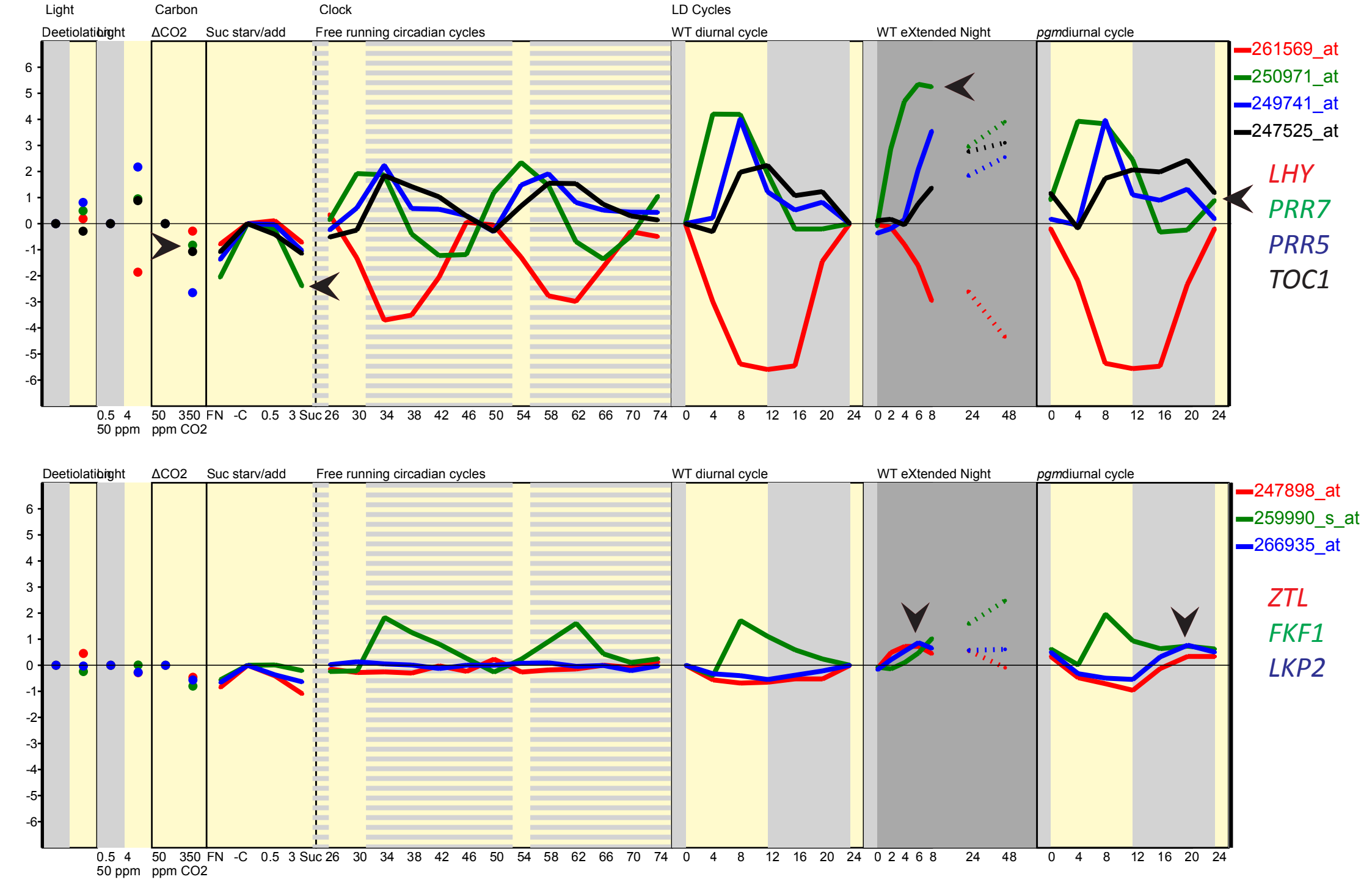
Light
Carbon
Clock
LD Cycles
Deetiolation
Light
ΔCO2
Suc starv/add
Free running circadian cycles
WT diurnal cycle
WT eXtended Night
pgmdiurnal cycle
261569_at
250971_at
249741_at
247525_at
LHY
PRR7
PRR5
TOC1
0.5 4
50 ppm
50 350
ppm CO2
FN -C 0.5 3 Suc
26 30 34 38 42 46 50 54 58 62 66 70 74
0 4 8 12 16 20 24
0 2 4 6 8 24 48
0 4 8 12 16 20 24
Deetiolation
Light
ΔCO2
Suc starv/add
Free running circadian cycles
WT diurnal cycle
WT eXtended Night
pgmdiurnal cycle
247898_at
259990_s_at
266935_at
ZTL
FKF1
LKP2
0.5 4
50 ppm
50 350
ppm CO2
FN -C 0.5 3 Suc
26 30 34 38 42 46 50 54 58 62 66 70 74
0 4 8 12 16 20 24
0 2 4 6 8 24 48
0 4 8 12 16 20 24

Supplementary Figure 7. Regulation of clock-related genes in low-sugar conditions.

RNA microarray data (Blasing *et al.*, 2005; Usadel *et al.*, 2008) displayed by the online tool (http://mapman.mpimp-golm.mpg.de/supplement/xn/) from treatments with light, CO_2-free air (ΔCO_2), DD (eXtended Night), or the starchless *pgm* mutant, for (A) *LHY*, *PRR7* (green), *PRR5* and *TOC1*; (B) *ZTL, FKF1* and *LKP2*. (A) Arrows mark higher *PRR7* levels in sugar-limiting DD and *pgm* relative to control in LD cycle, repression by re-supply of high exogenous sugar (3 Suc) but less effect from resupply of normal air (350ppm CO_2). (B) Arrows mark higher levels of *ZTL, FKF1* and *LKP2* RNA in DD and *pgm.*